

A Cahn-Hilliard Approach to Thermodiffusion in Porous Media

*Original*

A Cahn-Hilliard Approach to Thermodiffusion in Porous Media / Carfagna, Melania; Grillo, Alfio. - In: JOURNAL OF POROUS MEDIA. - ISSN 1091-028X. - 22:7(2019), pp. 761-785. [10.1615/JPorMedia.2019029077]

*Availability:*

This version is available at: 11583/2796636 since: 2020-05-11T21:18:05Z

*Publisher:*

Begell House

*Published*

DOI:10.1615/JPorMedia.2019029077

*Terms of use:*

This article is made available under terms and conditions as specified in the corresponding bibliographic description in the repository

*Publisher copyright*

(Article begins on next page)

# A Cahn-Hilliard Approach to Thermodiffusion in Porous Media

Melania Carfagna\*, Alfio Grillo†

DISMA “G.L. Lagrange”, Politecnico di Torino,  
C.so Duca degli Abruzzi 24, I-10129, Torino (TO) Italy

2019-6-23

## Abstract

We consider a fluid-saturated porous medium exposed to a non-uniform temperature field, and describe it as a non-isothermal biphasic mixture comprising a solid and a two-constituent fluid. We model such a system by assuming that the fluid free energy density depends on the gradient of the solute mass fraction. This constitutive choice induces a coupling between the temperature gradient and the solute diffusive mass flux, which adds itself to the standard Soret effect. We present numerical simulations of a thermogravitational cell to show how the modified constitutive framework, which is mandatory in diffuse-interface problems (e.g. the Cahn-Hilliard model), could lead to some novel interpretations of thermodiffusion, and enrich the phenomenological description of the considered benchmarks.

**Keywords:** Soret Effect, Thermodiffusion, Mixture Theory, Cahn-Hilliard Model.

**AMS Subject Classification:** 05A16, 65N38, 78M50.

---

\*melania.carfagna@polito.it

†Corresponding Author: Alfio Grillo (E-mail: [alfio.grillo@polito.it](mailto:alfio.grillo@polito.it)), C.so Duca degli Abruzzi 24, I-10129, Torino (TO), Italy.

# 1 Introduction

The onset of a mass flux by means of a thermal gradient is a phenomenon known as *thermodiffusion*, and its manifestation is said to be the Soret effect. Dually, the *Dufour effect* consists of the generation of a heat flux by means of the concentration gradient of a solute in a fluid solution. Such phenomena are referred to as *coupled phenomena* or *cross-effects*, as they represent the experimental evidence of the coupling between the flux of a given extensive quantity and the gradient of a state variable that is not directly power-conjugate to it (Bear and Bachmat, 1990). In the following, we shall be merely concerned with thermodiffusion and Soret effect.

In this work, we study a system comprising a porous medium and a two-constituent fluid that rearranges its composition under the action of a thermal gradient. In particular, we analyse two experiments in which an initially uniform fluid undergoes a separation of its constituents due to a mass flux initiated by a temperature gradient. Such experiments, performed by using a device known as thermogravitational cell, have been investigated, for example, by Jamet et al. (1992), Fargue et al. (1998), and Benano-Melly et al. (2001). In the experimental setting pertaining to the so-called *pure* Soret effect (Tyrrell, 1956), an initially uniform solution is put between two horizontal plates, kept at different temperatures. To reduce convection, the upper plate is held at a temperature higher than that of the lower one. Under these conditions, a stationary state can be attained, in which the thermal gradient balances the gradient of concentration. In the case of the thermogravitational cell, the fluid mixture is initially uniform, but the surfaces kept at different temperatures are vertical, which implies that the fluid velocity influences the mass transport of the mixture constituents by means of convection currents as well as solutal and thermal dispersion (Benano-Melly et al., 2001). We remark, however, that both in the description given by Tyrrell (1956) and in that provided by Benano-Melly et al. (2001), the common feature of thermodiffusion is the capability of developing a concentration gradient from an initially uniform mixture.

As second-order contributions, the Soret and Dufour effects are often disregarded. There are cases, however, in which they play an appreciable role. Ingle and Horne (1973)

and Rowley and Horne (1980) addressed thermal diffusion and the Dufour effect in mixtures of organic fluids of different composition. The Soret effect was observed in various physical frameworks, such as solar ponds (Celestino et al., 2006) and compact clays (Rosanne et al., 2001). Moreover, the thermally induced solutal separation has been investigated by several authors (Fargue et al., 1998; Zhang et al., 1999; Benano-Melly et al., 2001; Rauch and Köhler, 2002, 2003; Fargue et al., 2004; Grillo et al., 2011; Srinivasan and Saghir, 2013) both for organic and inorganic compounds. A review on experimental results about the Soret effect is provided by Platten (2006).

Thermodiffusion has attracted several scientists also in more recent times and, in fact, studies on Soret and Dufour effects in non-Darcy porous media have been conducted, for example, by RamReddy et al. (2016), Yadav and Kim (2015), Mallikarjuna et al. (2014), and Srinivasacharya et al. (2014). Soret and Dufour effects have also been investigated by Harinath Reddy et al. (2016) for the case of “*radiation absorption fluid*”, and by Chandra Shekar et al. (2016) for the case of magnetohydrodynamic “*natural convective heat and solute transfer*”. Moreover, Veeresh et al. (2016) analysed “*thermal diffusion effects in unsteady magnetohydrodynamic*” problems.

The theory of thermodiffusion constitutes an important chapter of Non-Equilibrium Thermodynamics. The mathematical apparatus on which it is developed relies on the Curie Principle and the Onsager-Casimir reciprocity relations (De Groot and Mazur, 1984; Bear and Bachmat, 1990). These are invoked to express the mass and heat fluxes as functions of both the gradient of temperature and the gradient of the solutal relative chemical potential.

In fact, thermodiffusion is the manifestation of a symmetry-breaking that occurs in a mixture exposed to a thermal gradient, with the system passing from a uniform to a non-uniform distribution of mass, and the separation of the mixture’s components being the most relevant effect of the non-uniformity of the chemical potential.

The main idea of our work is to capture the symmetry-breaking associated with the phenomenon of thermodiffusion in the constitutive formulation of the Helmholtz free energy density,  $\hat{A}_f$ , of a two-constituent fluid. To this end, we choose the mass fraction of

one of the constituents of the mixture as the order parameter of the system, and prescribe  $\hat{A}_f$  to be a function of all the state variables of the standard framework of thermodiffusion and of the gradient of the selected order parameter. In particular, we assume that  $\hat{A}_f$  is of the Cahn-Hilliard type.

The Cahn-Hilliard model was originally conceived for two-phase flows of non-miscible (or weakly miscible) fluids (Anderson and McFadden, 1998; Lowengrub and Truskinovsky, 1998). It is a mean-field approach that is able to describe also separation processes, which are driven by the presence of a superficial tension between the phases, culminating with the formation of a *diffuse interface* between two species. Such separation process can be affected also by the presence of a thermal field (Jasnow and Vinals, 1996). Choosing a Helmholtz free energy density of the Cahn-Hilliard type allows to account for end-wall effects and for the spatial resolution of the solutal mass fraction at the constitutive level, and induces a spontaneous coupling between mass diffusion and thermal gradients. We remark that this coupling stems from the constitutive framework, rather than being a consequence of the Curie Principle and Onsager's relations. From the theoretical viewpoint, its major consequence is the production of a non-standard Soret effect, which adds itself to the one of standard thermodiffusion. To quantify the relevance of our theoretical predictions, we reproduce numerically the experiments in a thermogravitational cell by enforcing both the standard and the non-standard (i.e., Cahn-Hilliard based) model of thermodiffusion. We show how the latter may be used as an additional tool for fitting experimental curves, thereby supplying a correction to the results obtained within the classical framework.

Although the Cahn-Hilliard model has been employed especially in the numerical treatment of two-fluid systems, there is an analogy between this higher order theory and the one developed in the framework of Mixture Theory. Indeed, the Cahn-Hilliard model describes the two-fluid system by means of the usual mass and momentum balance law of a single-fluid system, plus an evolution law for an *order parameter*, which in fact can be retrieved from the mass balance law of one of the two fluids, if it is regarded as a component of a binary mixture. This leads to the definition of two distinct regions,

each of which is occupied by one of the two fluids only, and a third region, the *diffuse interface*, whose characteristic dimensions should be smaller than the other two bulk domains. In the latter, the mixture model can be employed *tout court*, while in the other two, the order parameter acts as a weight, switching off those terms in the equations that pertain to the mixture description. From our understanding, in a two-fluid system, the explicit modelling of a diffuse interface could be done for two main reasons: (a) to avoid the numerical treatment of the discontinuities at the interface between the fluids, which pertains to the *sharp interface* models (Yue et al., 2004); (b) when the dynamical phenomena occurring in that layer influence the entire system, as in the case of an evident surface tension, or non negligible diffusion in the transition zone. Still, the mathematical introduction of a diffuse interface, arising in the Cahn-Hilliard model, has been used for miscible fluids in which dynamical effects that mimic the presence of an interfacial tension are, at least instantaneously, relevant (Joseph et al., 1996). This could be the case of a mixing problem, in which the Korteweg stress, i.e., an additional stress appearing in the momentum balance law of the whole system due to the presence of a gradient of composition, should be taken into account as a surface tension that vanishes as far as the mixing layer spreads (Davis, 1988). Moreover, a dedicated literature (Swernsath et al., 2010; Chen et al., 2017, 2015; Dias et al., 2010) introduces the effects of the Korteweg stress tensor also for treating the injection of miscible fluids in porous media, or in the case of unsaturated flow Cueto-Felgueroso et al. (2009).

Our study has been inspired by some discrepancies between the experimental and the numerical studies of the curves “separation ratio vs permeability” associated with a thermogravitational cell (Benano-Melly et al., 2001; Jamet et al., 1992; Fargue et al., 1998). Numerical results obtained within the classical framework of thermodiffusion were compared with the experimental ones by Jamet et al. (1992), and quite a relevant disagreement was noticed. It was observed that the evolution of the fluid in the thermogravitational cell is strongly influenced by the permeability and porosity of the porous medium (Jamet et al., 1992; Davarzani and Marcoux, 2011), by the characteristic dimension of the cell, the initial mass fraction of the solute, and the physico-chemical properties

of the mixture. Jamet et al. (1992) firstly attributed the discrepancy between the numerical and the experimental results to an anisotropic permeability. Subsequently, Benanome et al. (2001) considered also the effect of dispersion. Latest results are due to Nasrabadi et al. (2007), who showed that, by adding a compositional dependence of the Soret coefficient on the density (by means of a pressure dependent density), it is possible to obtain, at least for a binary mixture in a porous thermogravitational column, a good agreement between the experimental and numerical results, even though no further contribution of dispersion in the model is observed. The strong effect of the buoyancy term on the goodness of the results of the proposed classical models on thermodiffusion was also observed by Madariaga et al. (2011). For a non porous column (Thomaes cell), thermodiffusion is strongly affected by non trivial natural convection, which, in some cases (i.e., when the mean velocity of the mixture in the column is high), requires a full 3D treatment (Chavepeyer et al., 2002). A review has been given by Costeséque et al. (2002). Another fact concerns the *closure problem*, which could lead to a more or less realistic coarse scale approximation of the problem (effective thermodiffusion coefficients) (Quintard et al., 1997; Davarzani et al., 2010).

In the following, we show that adopting a Helmholtz free energy density of the Cahn-Hilliard type supplies a correction to the mass flux determined within the standard theory of thermodiffusion. Such a correction produces an additional coupling between the thermal gradient and the mass flux, and introduces a dispersive-like effect, which is related to the gradient of the solute mass fraction rather than to the fluid velocity. Although we are aware of the fact that the experimental set-up of the thermogravitational cell gives rise to convection currents, we focus here only on the effects associated with the use of a Helmholtz free energy density of the Cahn-Hilliard type. This may contribute to enrich the phenomenological picture of thermodiffusion and to stimulate alternative interpretations of the effects related to it.

The paper is structured as follows: In section 2, the mathematical model is developed in detail, and the Second Principle of Thermodynamics is exploited to determine consistent generalisations of the Fick and Darcy's laws in the context of Porous Media. In

section 3, we review the standard theory of thermodiffusion, and reformulate it within the Cahn-Hilliard framework. In section 4, we present the benchmark problems used for our numerical simulations, and introduce the employed numerical methods and model parameters. In section 5, we discuss in detail the obtained results, and validate our model by comparing its outputs with the experimental and numerical findings of other Authors. Particular care will be given to weighting the influence of the Cahn-Hilliard correction. Finally, in section 6, we summarise our results, and suggest some possible research topics.

## 2 Mathematical Model

We consider a physical system consisting of a two-constituent fluid,  $\mathcal{F}$ , and a porous medium,  $\mathcal{P}$ . The fluid is free to move throughout the void space of  $\mathcal{P}$ , and is assumed to saturate it completely. Due to the hypothesis of saturation, the porosity of  $\mathcal{P}$  coincides with the volumetric fraction of  $\mathcal{F}$ , denoted by  $\phi$ , and the volumetric fraction of  $\mathcal{P}$  is given by  $1 - \phi$ . At a sufficiently coarse scale of observation, the system under investigation can be studied by means of Hybrid Mixture Theory (Hassanizadeh, 1986; Bennethum et al., 2000). In this context,  $\mathcal{F}$  and  $\mathcal{P}$  can also be referred to as the fluid and solid phase, respectively.

We focus only on the case in which  $\mathcal{P}$  is rigid, at rest, and incompressible. In particular, its mass density,  $\varrho_s$ , is regarded as a given constant. Thus, the velocity of the solid porous medium,  $\mathbf{u}_s$ , is null at all times and all points. These assumptions, the mass balance law of the solid phase, and the saturation constraint imply that  $\phi$  is independent of time. In the sequel, we shall also assume that  $\phi$  is constant in space.

### 2.1 Balance laws

The mass balance law of the fluid phase,  $\mathcal{F}$ , is given by

$$\partial_t(\phi\varrho_f) + \operatorname{div}(\phi\varrho_f\mathbf{u}_f) = 0, \quad (1)$$



where  $\varrho_f$  is mass density and  $\mathbf{u}_f$  is the velocity of  $\mathcal{F}$ . Sometimes it is convenient to rewrite (1) in terms of the solid phase velocity,  $\mathbf{u}_s$ , and the relative velocity  $\mathbf{u}_{fs} \equiv \mathbf{u}_f - \mathbf{u}_s$ , which describes the motion of  $\mathcal{F}$  relative to  $\mathcal{P}$ . However, since the velocity of the solid phase is null in the present context, it holds that  $\mathbf{u}_{fs} = \mathbf{u}_f$ . We denote by  $\mathcal{C}_1$  and  $\mathcal{C}_2$  the constituents of the fluid phase, and select  $\mathcal{C}_1$  as the reference constituent. The composition of  $\mathcal{F}$  is determined by the mass fractions of  $\mathcal{C}_1$  and  $\mathcal{C}_2$ , which are indicated by  $c_1$  and  $c_2$ , respectively. Since it holds that  $c_1 + c_2 = 1$ , it suffices to determine the mass fraction of the reference constituent,  $c_1 \equiv c$ , to obtain also  $c_2 = 1 - c$ , and thus define the local amounts of  $\mathcal{C}_1$  and  $\mathcal{C}_2$  in  $\mathcal{F}$ . By introducing the velocity of  $\mathcal{C}_1$ ,  $\mathbf{u}_{1f}$ , and the relative velocity  $\mathbf{v} \equiv \mathbf{u}_{1f} - \mathbf{u}_f$ , the mass balance law of  $\mathcal{C}_1$  can be written as

$$\phi \varrho_f \dot{c} + \operatorname{div} \mathbf{J}_M = 0, \quad (2)$$

where  $\mathbf{J}_M \equiv \phi \varrho_f c \mathbf{v}$  is the mass flux vector associated with  $\mathcal{C}_1$ , while  $\dot{c} \equiv \partial_t c + \mathbf{u}_f \cdot \nabla c$  is the substantial derivative of  $c$  with respect to the velocity of  $\mathcal{F}$ . In addition to (1) and (2), also the balance laws of momentum, energy, and entropy have to be introduced. Following Hassanizadeh (1986), it can be shown that, if gravity is the only external force acting on the system, if inertial forces are negligible, and the relative velocities  $\mathbf{u}_{fs}$  and  $\mathbf{v}$  are sufficiently small (i.e.,  $\|\mathbf{u}_{fs}\|^2 \ll 1$  and  $\|\mathbf{v}\|^2 \ll 1$ ), the momentum balance laws of  $\mathcal{F}$  and  $\mathcal{C}_1$  reduce, respectively, to (Hassanizadeh, 1986)

$$\operatorname{div} \boldsymbol{\sigma} + \mathbf{m} + \phi \varrho_f \mathbf{g} = \mathbf{0}, \quad (3a)$$

$$\phi \varrho_f c \nabla \vartheta = \mathbf{f}. \quad (3b)$$

In (3a),  $\boldsymbol{\sigma}$  is the Cauchy stress tensor of the fluid phase,  $\mathbf{g}$  is the gravity acceleration vector, and  $\mathbf{m}$  represents the interaction forces exchanged between  $\mathcal{P}$  and  $\mathcal{F}$ . In (3b),  $\mathbf{f}$  is the dissipative part of the interaction forces exchanged between the two fluid constituents, and  $\vartheta \equiv \vartheta_1 - \vartheta_2$  is the relative chemical potential of  $\mathcal{C}_1$  with respect to  $\mathcal{C}_2$ , whereas  $\vartheta_1$  and  $\vartheta_2$  are the chemical potentials of the constituents  $\mathcal{C}_1$  and  $\mathcal{C}_2$ , respectively. Furthermore,

the energy balance law for the system as a whole can be written as

$$\phi \varrho_f T \dot{\eta}_f + (1 - \phi) \varrho_s T \partial_t \eta_s = -\operatorname{div} \mathbf{J}_Q - \phi \varrho_f \vartheta \dot{c} - \mathbf{m}_d \cdot \mathbf{u}_{fs}, \quad (4)$$

where  $T$  is absolute temperature,  $\eta_f$  and  $\eta_s$  are the entropy densities per unit mass of the fluid and the solid phase, respectively,  $\mathbf{J}_Q$  is referred to as the *effective* heat flux vector of the system, and  $\mathbf{m}_d$  is the dissipative part of  $\mathbf{m}$ . The balance laws (1)–(4) are completed with the Second Law of Thermodynamics, which, in the local form of the Clausius-Duhem inequality, requires the system’s overall entropy production,  $\Lambda$ , to be non-negative at all times and all points of the system, i.e.,  $\Lambda \geq 0$  (De Groot and Mazur, 1984).

## 2.2 Constitutive laws

The quantities  $\boldsymbol{\sigma}$ ,  $\mathbf{m}$ ,  $\mathbf{m}_d$ ,  $\vartheta$ ,  $\mathbf{f}$ ,  $\eta_f$ ,  $\eta_s$ , and  $\mathbf{J}_Q$  will be determined constitutively, and should thus comply with the condition  $\Lambda \geq 0$ . Our constitutive model is based on the theory developed by Hassanizadeh (1986) and Bennethum et al. (2000), and is then specialised to the problem at hand by enforcing the following further hypotheses (Grillo et al., 2011): (1). Radiative sources of energy and mass-exchange processes are excluded from the present study; (2). The fluid phase is macroscopically inviscid; (3). The mass density of  $\mathcal{F}$ ,  $\varrho_f$ , is an assigned constitutive function of the mass fraction,  $c$ , and absolute temperature,  $T$ , i.e., we set  $\varrho_f = \hat{\varrho}_f(c, T)$ ; (4). The physical processes relevant to the investigated problem necessitate the following list of independent constitutive variables  $\text{ICV} = \{T, c, \nabla T, \nabla c, \mathbf{u}_{fs}, \mathbf{v}\}$ . To provide an explicit mathematical expression of the quantities introduced so far, and of other constitutive variables necessary for the description of the system, we introduce the Helmholtz free energy densities of the solid and the fluid phase,  $A_s$  and  $A_f$ , and express them constitutively as  $A_s = \hat{A}_s(T)$  and  $A_f = \hat{A}_f(c, \nabla c, T)$ . Within this constitutive framework, the entropy densities of  $\mathcal{P}$  and  $\mathcal{F}$ , i.e.,  $\eta_s$  and  $\eta_f$ , the Cauchy stress tensor borne by  $\mathcal{F}$ ,  $\boldsymbol{\sigma}$ , and the Gibbs free energy density of the fluid phase,

231  $G_f$ , are given by:

$$\eta_s = -\frac{\partial \hat{A}_s}{\partial T}, \quad (5a)$$

$$\eta_f = -\frac{\partial \hat{A}_f}{\partial T} + \frac{p}{\varrho_f^2} \frac{\partial \hat{\varrho}_f}{\partial T} = -\frac{\partial \hat{G}_f}{\partial T}, \quad (5b)$$

$$\boldsymbol{\sigma} = -\phi p \mathbf{I} - \nabla c \otimes \left( \phi \varrho_f \frac{\partial \hat{G}_f}{\partial \nabla c} \right), \quad (5c)$$

$$G_f = \hat{G}_f(c, \nabla c, T, p) = \hat{A}_f(c, \nabla c, T) + \frac{p}{\hat{\varrho}_f(c, T)}, \quad (5d)$$

232 where  $p$  is the fluid pressure,  $\mathbf{I}$  is the second-order identity tensor, and the non-hydrostatic  
233 contribution

$$\boldsymbol{\sigma}_K \equiv -\nabla c \otimes \left( \phi \varrho_f \frac{\partial \hat{G}_f}{\partial \nabla c} \right) \quad (6)$$

234 is the Korteweg stress tensor. Furthermore, the relative chemical potential,  $\vartheta$ , reads

$$\begin{aligned} \vartheta &= \left( \frac{\partial \hat{A}_f}{\partial c} - \frac{p}{\varrho_f^2} \frac{\partial \hat{\varrho}_f}{\partial c} \right) - \frac{1}{\phi \varrho_f} \operatorname{div} \left( \phi \varrho_f \frac{\partial \hat{A}_f}{\partial \nabla c} \right) \\ &= \frac{\partial \hat{G}_f}{\partial c} - \frac{1}{\phi \varrho_f} \operatorname{div} \left( \phi \varrho_f \frac{\partial \hat{G}_f}{\partial \nabla c} \right). \end{aligned} \quad (7)$$

235 Finally, by introducing the system's heat flux vector,  $\mathbf{q}$ , and the entropy flux vector

$$\mathbf{q}_\eta \equiv \frac{\mathbf{q}}{T} + \frac{1}{T} \left( \phi \varrho_f \frac{\partial \hat{A}_f}{\partial \nabla c} \right) \dot{c} = \frac{\mathbf{q}}{T} + \frac{1}{T} \left( \phi \varrho_f \frac{\partial \hat{G}_f}{\partial \nabla c} \right) \dot{c}, \quad (8)$$

236 the effective heat flux vector  $\mathbf{J}_Q$  is written as  $\mathbf{J}_Q \equiv T \mathbf{q}_\eta$ . The presence of  $\nabla c$  among the  
237 arguments of  $\hat{G}_f$ , cf. (5d), implies that  $\mathbf{q}_\eta$  cannot be written as the ratio between the  $\mathbf{q}$   
238 and  $T$ , as is the case in standard Continuum Thermodynamics (Mićunović, 2009; Gurtin  
239 et al., 2010). Nevertheless, by construction it does hold that  $\mathbf{q}_\eta = \mathbf{J}_Q/T$ .

240 A well-known model, constructed upon a free energy density depending on a scalar  
241 field and its gradient, is the Cahn-Hilliard model (cf., for example, (Gurtin, 1996) for a  
242 review). It describes the evolution of a two-phase system, in which the distribution of  
243 the phases is represented by a scalar order parameter, and the free energy is written as  
244 the sum of a contribution depending on the order parameter only, and a contribution

depending on the gradient of the order parameter. The order parameter solves a mass diffusion equation, in which the mass diffusive flux depends linearly on the gradient of the chemical potential of the diffusing substance. In this context, the chemical potential is the functional derivative of the system's free energy.

Since in our work mass diffusion plays a central role, our thermodynamic model is grounded on the Cahn-Hilliard theory. For this purpose, we consider a Helmholtz free energy density of the Cahn-Hilliard type, given by

$$\hat{A}_f(c, \nabla c, T) = \hat{A}_{st}(c, T) + \frac{1}{2}\lambda \|\nabla c\|^2, \quad (9)$$

where  $\hat{A}_{st}(c, T)$  may be referred to as the *standard* Helmholtz free energy density, and  $\lambda$  is a coefficient having the meaning of a mixing free energy. By plugging (9) into (5d), the Gibbs free energy density becomes

$$\hat{G}_f(c, \nabla c, T, p) = \hat{G}_{st}(c, T, p) + \frac{1}{2}\lambda \|\nabla c\|^2, \quad (10)$$

where the standard part,  $\hat{G}_{st}(c, T, p)$ , is given by

$$\hat{G}_{st}(c, T, p) = \hat{A}_{st}(c, T) + \frac{p}{\hat{\varrho}_f(c, T)}. \quad (11)$$

Also the chemical potential,  $\vartheta$ , can be written as  $\vartheta = \vartheta_{st} + \vartheta_{CH}$ , where

$$\vartheta_{st} = \frac{\partial \hat{G}_f}{\partial c} = \frac{\partial \hat{G}_{st}}{\partial c}, \quad (12a)$$

$$\vartheta_{CH} = -\frac{1}{\phi \varrho_f} \operatorname{div} \left( \phi \varrho_f \frac{\partial \hat{G}_f}{\partial \nabla c} \right) = -\frac{1}{\phi \varrho_f} \operatorname{div} (\phi \varrho_f \lambda \nabla c). \quad (12b)$$

We refer to  $\vartheta_{st}$  and  $\vartheta_{CH}$  as to the *standard* and the *Cahn-Hilliard* chemical potential, respectively. The standard part of the Gibbs free energy of the fluid phase,  $\mathcal{F}$ , can be written as

$$\hat{G}_{st}(c, T, p) = c \hat{\vartheta}_{st1}(c, T, p) + (1 - c) \hat{\vartheta}_{st2}(c, T, p), \quad (13)$$

where

$$\hat{\vartheta}_{\text{st1}}(c, T, p) = \frac{RT}{M_1} \log \left[ \frac{cM_2}{(1-c)M_1 + cM_2} \right] + \alpha_1(T)p + \beta(T), \quad (14a)$$

$$\hat{\vartheta}_{\text{st2}}(c, T, p) = \frac{RT}{M_2} \log \left[ \frac{(1-c)M_1}{(1-c)M_1 + cM_2} \right] + \alpha_2(T)p + \beta(T), \quad (14b)$$

are the standard chemical potentials associated with the constituents  $\mathcal{C}_1$  and  $\mathcal{C}_2$  of  $\mathcal{F}$ , respectively,  $R$  is the gas constant,  $M_1$  and  $M_2$  are the molar masses of  $\mathcal{C}_1$  and  $\mathcal{C}_2$ , and  $\alpha_1(T)$ ,  $\alpha_2(T)$ , and  $\beta(T)$  are given functions of the temperature. We remark that  $\hat{\vartheta}_{\text{st1}}$  and  $\hat{\vartheta}_{\text{st2}}$  are consistent with the equality

$$c \frac{\partial \hat{\vartheta}_{\text{st1}}}{\partial c} + (1-c) \frac{\partial \hat{\vartheta}_{\text{st2}}}{\partial c} = 0. \quad (15)$$

When the Cahn-Hilliard model is used to describe binary systems comprising two non-miscible fluids, the term  $\frac{1}{2}\lambda\|\nabla c\|^2$  introduces a partial miscibility regularisation (Lowengrub and Truskinovsky, 1998), and  $\lambda$  is referred to as the capillarity coefficient (Jamet, 2001). In this case,  $\lambda$  should be supplied constitutively. However, it is possible to determine  $\lambda$  by having recourse to the definition of *Cahn number* (Choi and Anderson, 2012; Lowengrub and Truskinovsky, 1998). Hence, we may set  $\lambda = CL^2\vartheta_{\text{ref}}$ , where  $L$  is the characteristic length of the computational domain,  $\vartheta_{\text{ref}}$  is a referential, characteristic chemical potential, and  $C \equiv \xi/L$  is the Cahn number, i.e., the ratio between the characteristic meso-scale length  $\xi$ , which represents the interface width, and  $L$ . Despite these considerations, in all the forthcoming numerical simulations,  $\lambda$  will be taken equal to a constant known from the outset.

## 2.3 Entropy production

The constitutive relations (5)–(7) allow to obtain an explicit expression for the rate of overall entropy production,  $\Lambda$ , which is equal to the ratio between the overall power

279 dissipated by system and the absolute temperature (Grillo et al., 2011), i.e.,

$$\Lambda = -\frac{\mathbf{m}_d \cdot \mathbf{u}_{fs}}{T} - \frac{\nabla \vartheta \cdot \mathbf{J}_M}{T} - \frac{\nabla T \cdot (\mathbf{J}_Q - \vartheta \mathbf{J}_M)}{T^2} \geq 0. \quad (16)$$

280 In this work, we admit that the dynamic regime of the fluid phase is compatible with  
 281 Darcy's law. Thus, we express the dissipative force  $\mathbf{m}_d$ , which is defined by  $\mathbf{m}_d \equiv \mathbf{m} - p \nabla \phi$   
 282 (Hassanizadeh, 1986), as a linear constitutive function of the filtration velocity  $\mathbf{w} \equiv$   
 283  $\phi \mathbf{u}_{fs}$ , i.e., we set  $\mathbf{m}_d = -\mathbf{r} \mathbf{w}$ , where  $\mathbf{r}$  is a second-order tensor referred to as resistivity  
 284 tensor. Here, we assume that  $\mathbf{r}$  is symmetric and positive-definite. By accounting for the  
 285 definitions (5c) and (6), we solve (3a) with respect to  $\mathbf{w}$ , thereby obtaining

$$\mathbf{w} = -\frac{\mathbf{k}}{\mu} \left[ (\nabla p - \varrho_f \mathbf{g}) - \frac{1}{\phi} \operatorname{div} \boldsymbol{\sigma}_K \right], \quad (17)$$

286 where  $\mathbf{k}$  is the permeability tensor,  $\mu$  is the dynamic viscosity of the fluid, and the identity  
 287  $\phi \mathbf{r}^{-1} = \mathbf{k} / \mu$  has been used. Equation (17) is a generalisation to Darcy's law in which the  
 288 divergence of the Korteweg stress tensor contributes to the fluid filtration velocity. By  
 289 computing  $\boldsymbol{\sigma}_K$  explicitly, and recalling that  $\phi$  is assumed to be constant throughout this  
 290 work, we obtain  $-\phi^{-1} \operatorname{div} \boldsymbol{\sigma}_K = \operatorname{div}(\varrho_f \lambda \nabla c \otimes \nabla c)$ . If the variability of  $\varrho_f$  is neglected, this  
 291 expression takes on the form (Collins et al., 2013; Diegel et al., 2015)

$$-\phi^{-1} \operatorname{div} \boldsymbol{\sigma}_K = \operatorname{div}(\varrho_f \lambda \nabla c \otimes \nabla c) = \varrho_f \lambda (\nabla \nabla c) \nabla c - \varrho_f \vartheta_{CH} \nabla c, \quad (18)$$

292 where  $\vartheta_{CH} = -\lambda \Delta c$  is the Cahn-Hilliard chemical potential (12b), obtained under the  
 293 hypotheses that  $\phi$ ,  $\varrho_f$ , and  $\lambda$  are constants. Since  $\mathbf{r}$  is positive-definite, the first term on  
 294 the right-hand-side of (16) is always non-negative, i.e.,

$$\Lambda_F \equiv -\frac{\mathbf{m}_d \cdot \mathbf{u}_{fs}}{T} = \frac{\mathbf{r} : (\mathbf{w} \otimes \mathbf{w})}{\phi T} \geq 0, \quad \forall \mathbf{w}, \quad (19)$$

295 where  $\Lambda_F$  is the part of the overall rate of entropy production associated with the fluid  
 296 flow. Equation (19) implies that, to satisfy the inequality (16), it is sufficient to require  
 297 that the part of  $\Lambda$  due to mass diffusion and heat conduction, denoted by  $\Lambda_{MQ}$  hereafter,

has to be non-negative. This requirement can be put in one of the two equivalent forms

$$\Lambda_{\text{MQ}} = -\frac{\nabla\vartheta \cdot \mathbf{J}_{\text{M}}}{T} - \frac{\nabla T \cdot (\mathbf{J}_{\text{Q}} - \vartheta \mathbf{J}_{\text{M}})}{T^2} \geq 0, \quad (20\text{a})$$

$$\Lambda_{\text{MQ}} = -\mathbf{J}_{\text{M}} \cdot \nabla \left( \frac{\vartheta}{T} \right) - \mathbf{J}_{\text{Q}} \cdot \frac{\nabla T}{T^2} \geq 0, \quad (20\text{b})$$

and is enforced in order to extract constitutive information on the heat flux vector  $\mathbf{J}_{\text{Q}}$  and on the mass diffusive flux vector  $\mathbf{J}_{\text{M}}$ .

### 3 Thermodiffusion

In spite of the fact that (20a) and (20b) are interchangeable representations of  $\Lambda_{\text{MQ}}$ , selecting one of these two possible forms has repercussions on the constitutive expressions of the fluxes  $\mathbf{J}_{\text{M}}$  and  $\mathbf{J}_{\text{Q}}$  and on the interpretation of the phenomenological coefficients featuring in these expressions. A thorough review on this issue was written by De Groot and Mazur (1984). In this work, we adhere to the formulation given in (20b) (cf. De Groot and Mazur (1984), Ch. 5, Sec. 3, p. 49).

#### 3.1 Standard thermodiffusion

In this section, we make a brief review on standard thermodiffusion. For this purpose, we take a step backwards and consider the thermodynamic framework in which the Helmholtz free energy density of the fluid phase is a function of  $c$  and  $T$  only, i.e.,  $A_{\text{f}} = \hat{A}_{\text{f}}(c, T) \equiv \hat{A}_{\text{st}}(c, T)$ . When this is the case, the relative chemical potential reduces to the standard one, i.e.,  $\vartheta = \vartheta_{\text{st}}$ , and  $\Lambda_{\text{MQ}}$  becomes

$$\Lambda_{\text{MQ}} = -\mathbf{J}_{\text{M}} \cdot \nabla \left( \frac{\vartheta_{\text{st}}}{T} \right) - \mathbf{J}_{\text{Q}} \cdot \frac{\nabla T}{T^2} \geq 0. \quad (21)$$

Hence, within the linear theory of the phenomenological laws for isotropic media, the fluxes  $\mathbf{J}_{\text{M}}$  and  $\mathbf{J}_{\text{Q}}$  are connected with the gradients  $-\nabla(\vartheta_{\text{st}}/T)$  and  $-(\nabla T)/T^2 = \nabla(1/T)$

through the formulae (De Groot and Mazur, 1984; Rauch, 2006)

$$\mathbf{J}_M = -L_{MM} \nabla \left( \frac{\vartheta_{\text{st}}}{T} \right) - L_{MQ} \frac{\nabla T}{T^2}, \quad (22a)$$

$$\mathbf{J}_Q = -L_{QM} \nabla \left( \frac{\vartheta_{\text{st}}}{T} \right) - L_{QQ} \frac{\nabla T}{T^2}, \quad (22b)$$

where  $L_{MM}$ ,  $L_{MQ}$ ,  $L_{QM}$ , and  $L_{QQ}$  are scalar phenomenological coefficients, constrained to satisfy Onsager's reciprocal relations  $L_{MQ} = L_{QM}$ . By working out the gradient of  $\vartheta_{\text{st}}/T$ , splitting the gradient of  $\vartheta_{\text{st}}$ , and introducing the specific relative enthalpy  $h_{\text{st}}$ , i.e.,

$$\nabla \vartheta_{\text{st}} = \nabla_T \vartheta_{\text{st}} + \frac{\partial \vartheta_{\text{st}}}{\partial T} \nabla T, \quad (23a)$$

$$h_{\text{st}} \equiv \vartheta_{\text{st}} - T \frac{\partial \vartheta_{\text{st}}}{\partial T}, \quad (23b)$$

the expressions of  $\mathbf{J}_M$  and  $\mathbf{J}_Q$  become

$$\mathbf{J}_M = -\frac{L_{MM}}{T} \nabla_T \vartheta_{\text{st}} - (L_{MQ} - h_{\text{st}} L_{MM}) \frac{\nabla T}{T^2}, \quad (24a)$$

$$\mathbf{J}_Q = -\frac{L_{QM}}{T} \nabla_T \vartheta_{\text{st}} - (L_{QQ} - h_{\text{st}} L_{QM}) \frac{\nabla T}{T^2}. \quad (24b)$$

The partial gradient  $\nabla_T \vartheta_{\text{st}}$  is obtained by holding temperature fixed and differentiating with respect to all other state variables. Since it follows from (12a) that  $\vartheta_{\text{st}}$  depends on the mass fraction,  $c$ , temperature,  $T$ , and pressure,  $p$ , i.e.,  $\vartheta_{\text{st}} = \hat{\vartheta}_{\text{st}}(c, T, p)$ , it holds that

$$\nabla_T \vartheta_{\text{st}} = \frac{\partial \hat{\vartheta}_{\text{st}}}{\partial c} \nabla c + \frac{\partial \hat{\vartheta}_{\text{st}}}{\partial p} \nabla p. \quad (25)$$

Substituting the second term on the right-hand-side of (25) into (24a) and (24b) leads to the baro-diffusion factor (Landau and Lifschitz, 1984)  $k_p \equiv p \frac{\partial \hat{\vartheta}_{\text{st}} / \partial p}{\partial \hat{\vartheta}_{\text{st}} / \partial c}$ , which vanishes identically for  $c = 0$  and  $c = 1$ . Since the baro-diffusion factor usually has a negligible influence on the fluxes  $\mathbf{J}_M$  and  $\mathbf{J}_Q$ , we approximate  $\nabla_T \vartheta_{\text{st}}$  with the first summand on the



right-hand-side of (25). Furthermore, by introducing the quantities

$$D \equiv \frac{1}{\varrho_f} \frac{L_{MM}}{T} \frac{\partial \hat{\vartheta}_{st}}{\partial c}, \quad (26a)$$

$$S_{st} \equiv \frac{1}{(1-c)c} \frac{L_{MQ}/L_{MM} - h_{st}}{T(\partial \hat{\vartheta}_{st}/\partial c)}, \quad (26b)$$

$$Q \equiv \frac{L_{QM}}{L_{MM}}, \quad (26c)$$

$$\kappa \equiv \frac{L_{QQ}}{T^2}, \quad (26d)$$

we recast (24a) and (24b) in the form

$$\mathbf{J}_M = -\varrho_f D [\nabla c + S_{st} c (1-c) \nabla T], \quad (27a)$$

$$\mathbf{J}_Q = -\varrho_f D Q \nabla c - \left( \kappa - h_{st} \frac{\varrho_f D Q}{T(\partial \hat{\vartheta}_{st}/\partial c)} \right) \nabla T. \quad (27b)$$

In (26a)–(26d),  $D$  and  $S_{st}$  are the diffusion coefficient and the standard Soret coefficient, respectively,  $Q$  is the *heat of transport*, and  $\kappa$  is the thermal conductivity (De Groot and Mazur, 1984; Rowley and Horne, 1980). Due to the symmetry requirement  $L_{MQ} = L_{QM}$ ,  $S_{st}$  and  $Q$  must satisfy the relation (Rauch, 2006; Grillo et al., 2011)

$$(1-c)c \frac{\partial \hat{\vartheta}_{st}}{\partial c} T S_{st} = Q - h_{st}. \quad (28)$$

Within the considered constitutive framework, the specific relative enthalpy,  $h_{st}$ , is usually neglected. This is particularly the case when the fluid phase is regarded as incompressible, or when the Boussinesq-Oberbeck approximation is invoked. Finally, although appreciable for some physical processes (Ingle and Horne, 1973), in the present work we claim that the contribution of the Dufour effect to the overall heat flux vector is negligible. Thus, we approximate  $\mathbf{J}_Q$  with standard Fourier's law, i.e., from here on we set

$$\mathbf{J}_Q = -\kappa \nabla T. \quad (29)$$

## 3.2 Thermodiffusion within the Cahn-Hilliard framework

In this section, we highlight the implications brought about by the use of a Gibbs free energy density of the Cahn-Hilliard type. For our purposes, we consider the expression of the residual rate of entropy production given in (20b) and, by adopting the same argument as in section 3.1, we express the fluxes  $\mathbf{J}_M$  and  $\mathbf{J}_Q$  as

$$\mathbf{J}_M = -L_{MM} \nabla \left( \frac{\vartheta}{T} \right) - L_{MQ} \frac{\nabla T}{T^2}, \quad (30a)$$

$$\mathbf{J}_Q = -L_{QM} \nabla \left( \frac{\vartheta}{T} \right) - L_{QQ} \frac{\nabla T}{T^2}. \quad (30b)$$

We do not speculate on  $\mathbf{J}_Q$  any further, since it will be approximated as in (29) in the sequel.

Rather, we work out (30a), which can be rewritten as

$$\begin{aligned} \mathbf{J}_M &= -L_{MM} \nabla \left( \frac{\vartheta_{st} + \vartheta_{CH}}{T} \right) - L_{MQ} \frac{\nabla T}{T^2} \\ &= -L_{MM} \nabla \left( \frac{\vartheta_{st}}{T} \right) - L_{MM} \nabla \left( \frac{\vartheta_{CH}}{T} \right) - L_{MQ} \frac{\nabla T}{T^2}. \end{aligned} \quad (31)$$

According to the procedure shown in section 3.1, and recalling (26a) and (26b), we obtain

$$\begin{aligned} \mathbf{J}_M &= -\varrho_f D [\nabla c + S_{st} c (1 - c) \nabla T] \\ &\quad + \varrho_f D \frac{\vartheta_{CH}}{T (\partial \hat{\vartheta}_{st} / \partial c)} \nabla T - \frac{\varrho_f D}{\partial \hat{\vartheta}_{st} / \partial c} \nabla \vartheta_{CH}. \end{aligned} \quad (32)$$

From here on, we call Cahn-Hilliard “*Soret coefficient*” the quantity

$$S_{CH} := \frac{-\vartheta_{CH}}{(1 - c) c T (\partial \hat{\vartheta}_{st} / \partial c)}. \quad (33)$$

This definition allows to rephrase the expression of the mass flux vector  $\mathbf{J}_M$  as

$$\mathbf{J}_M = -\varrho_f D [\nabla c + (S_{st} + S_{CH}) c (1 - c) \nabla T] - \frac{\varrho_f D}{\partial \hat{\vartheta}_{st} / \partial c} \nabla \vartheta_{CH}. \quad (34)$$

We define *effective Soret coefficient* the sum  $S_{\text{eff}} \equiv S_{st} + S_{CH}$ . According to (34), the inclusion of the Cahn-Hilliard theory into the standard framework of thermodiffusion

yields two corrections of the mass flux vector,  $\mathbf{J}_M$ . These manifest themselves through the additional “Soret coefficient”,  $S_{CH}$ , which is generated by the Cahn-Hilliard relative chemical potential,  $\vartheta_{CH}$ , and a term proportional to the gradient of  $\vartheta_{CH}$ . We remark that, while the standard Soret coefficient,  $S_{st}$  (which is typically expressed constitutively as a function of temperature and mass fraction), can be either positive or negative, and its sign may change in response to changes of mass fraction and temperature (Kita et al., 2004), the sign of  $S_{CH}$  depends essentially on the sign of  $\vartheta_{CH}$ . Since  $\phi$  is assumed to be constant in this work, and the Boussinesq-Oberbeck approximation will be enforced (i.e.,  $\rho_f$  will be regarded as constant everywhere, except in the buoyancy term,  $\rho_f \mathbf{g}$ , of Darcy’s law (17)),  $\vartheta_{CH}$  reduces to  $\vartheta_{CH} = -\text{div}(\lambda \nabla c) = -\lambda \Delta c$  (see (12b)). Thus, the sign of  $\vartheta_{CH}$  changes in space and time according to the sign of the Laplacian of the mass fraction.

## 4 Benchmark problems

As stated in the Introduction, a typical framework in which thermodiffusive effects are accounted for is the thermally induced separation of the components of a two-constituent mixture in response to the combined action of a thermal gradient and density-driven fluid flow. Hereafter, we employ a Finite Element model to reproduce numerically two experiments of thermally induced separation in a thermogravitational cell (Benano-Melly et al., 2001; Costeséque et al., 2002; Jamet et al., 1992). In both experiments, a thermogravitational cell of length  $L$  and width  $H = hL$  ( $h$  is a positive real number smaller than unity) is used, in which a porous medium with uniform and constant porosity  $\phi$  is saturated by a two-constituent fluid. The fluid is prepared in such a way that, at the initial time of observation, the mass fractions of its constituents are uniformly distributed. In the course of time, however, a separation process occurs, thereby leading to a slightly nonuniform distribution of the mass fractions within the cell. In the first experiment, the employed fluid is a mixture of pure water and heavy water (hereafter referred to as HDO) in a porous matrix of aluminium oxide,  $\text{Al}_2\text{O}_3$  (Benano-Melly et al., 2001; Costeséque et al., 2002). The second experiment adopts a mixture of tetracosane,  $\text{C}_{24}\text{H}_{50}$ , and dodecane,

$\text{C}_{12}\text{H}_{26}$ , (Jamet et al., 1992; Fargue et al., 1998). In the following, the constituent  $\mathcal{C}_1$ , whose mass fraction,  $c$ , features in the model equations, will be assumed to be HDO in the first experiment, and  $\text{C}_{24}\text{H}_{50}$  in the second one.

## 4.1 Summary of the model equations

The mathematical model considered in this work is based on the mass balance laws (1) and (2), and on the energy balance law (4). These are three scalar equations in the three unknowns represented by pressure,  $p$ , mass fraction,  $c$ , and temperature,  $T$ . The model is closed since  $\mathbf{w}$ ,  $\mathbf{J}_Q$ , and  $\mathbf{J}_M$  are specified in (17), (29), and (34), respectively, while  $\eta_s$ ,  $\eta_f$ , and  $\vartheta$  are prescribed in (5a), (5b), and (7), respectively.

To reduce the computational complexity of the model equations, which are highly coupled and non-linear, we enforce the Boussinesq-Oberbeck approximation. Accordingly, the mass density of the fluid phase is expressed as a function of  $c$  and  $T$  only in the buoyancy term of Darcy's law, i.e., in  $\varrho_f \mathbf{g} = \hat{\varrho}_f(c, T) \mathbf{g}$ , and is set equal to a reference constant,  $\varrho_0$ , everywhere else. Moreover, we neglect the Korteweg stress tensor,  $\boldsymbol{\sigma}_K$ , in the generalised Darcy's law (17), and the term  $\mathbf{m}_d \cdot \mathbf{u}_{fs} = -\phi^{-1} \mathbf{r} \mathbf{w} \cdot \mathbf{w}$  in (4). The latter simplification is done under the assumption that the terms of order higher than the first in  $\mathbf{w}$  are not significant in the present study.

Substituting the expression of  $\mathbf{J}_M$ , given in (34), into (2) leads to an equation that involves the derivatives of the mass fraction up to the fourth order. This is due to the fact that  $\mathbf{J}_M$  features the gradient of the Cahn-Hilliard chemical potential,  $\vartheta_{CH}$ , which, in turn, contains the derivatives of  $c$  up to the second order. Rather than following this approach, we treat  $\vartheta_{CH}$  as an additional unknown of the model, and determine  $c$  consistently with the constitutive relation (12b), which becomes  $\vartheta_{CH} = -\text{div}(\lambda \nabla c)$  due to the considered approximations, and is solved together with the balance laws. Thus, the model equations

take on the form

$$\operatorname{div}(\varrho_0 \mathbf{w}) = 0, \quad (35a)$$

$$\phi \varrho_0 \dot{c} + \operatorname{div} \mathbf{J}_M = 0, \quad (35b)$$

$$\vartheta_{CH} = -\operatorname{div}(\lambda \nabla c), \quad (35c)$$

$$C_{\text{eff}} \partial_t T + \operatorname{div}(\varrho_0 C_{\text{pf}} T \mathbf{w}) = \operatorname{div}(\kappa \nabla T) - \phi \varrho_0 \vartheta_{CH} \dot{c}, \quad (35d)$$

where  $\mathbf{w}$  is now given by standard Darcy's law, i.e.,

$$\mathbf{w} = -\frac{\mathbf{k}}{\mu} (\nabla p - \hat{\varrho}_f(c, T) \mathbf{g}), \quad (36)$$

$C_{\text{eff}}$  is referred to as the effective thermal capacity of the fluid-solid mixture, i.e.,

$$C_{\text{eff}} = \phi \varrho_0 C_{\text{pf}} + (1 - \phi) \varrho_s C_{\text{ps}}, \quad (37)$$

while  $C_{\text{pf}}$  and  $C_{\text{ps}}$  are the specific heats at constant pressure of the fluid and solid phase, respectively. Both are assumed to be constant in the present framework.

It is worth to remark that, with respect to a standard problem of thermodiffusion, there are two relevant differences. The first difference is related to the introduction of the Cahn-Hilliard ‘‘Soret coefficient’’,  $S_{CH}$  [cf. (33)], and the second one is due to the contribution  $\nabla \vartheta_{CH}$  to the overall mass flux vector  $\mathbf{J}_M$ . The presence of these two non-standard terms requires a special numerical treatment.

Notice that the additional term in the energy balance law (35d) could be split into two terms: the divergence of an additional flux  $\operatorname{div}(\vartheta_{CH} \mathbf{J}_M)$ , directed in the sense of the mass flux, which in our case is negligible ( $\simeq 1 \cdot 10^{-6}$  W/m<sup>2</sup>) compared to the conductive ( $\simeq 1 \cdot 10^5$  W/m<sup>2</sup>) and the convective ( $\simeq 1 \cdot 10^2$  W/m<sup>2</sup>) fluxes; a term  $-\mathbf{J}_M \cdot \nabla \vartheta_{CH}$  that reminds of an energy loss due to the mass exchange, whose order of magnitude is even smaller ( $\simeq 1 \cdot 10^{-9}$  W/m<sup>3</sup>).

Equations (35a)–(35d) apply in an open set  $\Omega \subset \mathbb{R}^d$ , with  $d = 2$  or  $d = 3$ , which constitutes the computational domain. The boundary of the cell,  $\partial\Omega$ , is assumed to be

impervious, i.e., no-flux conditions are imposed to the filtration velocity,  $\mathbf{w}$ , and the mass flux vector,  $\mathbf{J}_M$ , on all parts of  $\partial\Omega$ . The lower and the upper boundaries,  $\Gamma_l$  and  $\Gamma_u$ , are assumed to be thermally insulated, while the lateral boundaries,  $\Gamma_c$  and  $\Gamma_h$ , are kept at constant temperatures. In formulae, the set of boundary conditions read:

$$T|_{\Gamma_c} = T_c, \quad T|_{\Gamma_h} = T_h, \quad (38a)$$

$$\mathbf{J}_Q \cdot \mathbf{n} = 0, \quad \text{on } \Gamma_l \cup \Gamma_u, \quad (38b)$$

$$\mathbf{J}_M \cdot \mathbf{n} = 0, \quad \text{on } \partial\Omega, \quad (38c)$$

$$\mathbf{w} \cdot \mathbf{n} = 0, \quad \text{on } \partial\Omega, \quad (38d)$$

where  $\mathbf{n}$  is the unit vector normal to  $\partial\Omega$ , and  $T_c < T_h$ . In addition to (38a)–(38d), we also impose

$$-\lambda \nabla \vartheta_{CH} \cdot \mathbf{n} = 0, \quad \text{on } \partial\Omega, \quad (39)$$

thereby requiring that  $\vartheta_{CH}$  satisfies homogeneous Neumann conditions on the whole boundary of the thermogravitational cell.

In the standard numerical treatment of the Cahn-Hilliard model, it is rather customary to set the normal derivative of the total chemical potential equal to zero at the boundary of the computational domain, i.e.,  $\partial_n \vartheta = \nabla \vartheta \cdot \mathbf{n} = 0$ , on  $\partial\Omega$ , and to impose some “wetting angle condition” on  $\partial\Omega$  (Diegel et al., 2015; Jamet, 2001; Zhang et al., 1999). Within our framework, the latter condition is a consequence of (38c), and is expressed through a restriction on the normal derivative of the solutal concentration,  $\partial_n c = \nabla c \cdot \mathbf{n}$ , which has to hold on  $\partial\Omega$ . We emphasise, however, that  $\partial_n c$  need not be zero in our approach. Rather, in order to guarantee the solvability of the formulated mathematical problem, it is only required to satisfy some auxiliary constraint on  $\partial\Omega$ . In this sense, we speak in our work of a “generalised wetting condition”.

In the present study, the combination of (38b), (38c), and (39) implies the boundary condition  $\partial_n \vartheta = 0$  as well as the “wetting condition”,  $\partial_n c = 0$ , on  $\Gamma_l \cup \Gamma_u$ . This is due to the fact that Fourier’s law (29) prescribes the equality  $\mathbf{J}_Q = -\kappa \nabla T$ , and (38b) becomes  $\mathbf{J}_Q \cdot \mathbf{n} = -\kappa \nabla T \cdot \mathbf{n} = 0$  on  $\Gamma_l \cup \Gamma_u$ , thereby yielding  $\nabla T \cdot \mathbf{n} = 0$  on  $\Gamma_l \cup \Gamma_u$ . Hence, the

boundary condition (38c) reads

$$\mathbf{J}_M \cdot \mathbf{n} = -\frac{L_{MM}}{T} \nabla \vartheta \cdot \mathbf{n} = -\frac{L_{MM}}{T} (\nabla \vartheta_{st} \cdot \mathbf{n} + \nabla \vartheta_{CH} \cdot \mathbf{n}) = 0, \quad \text{on } \Gamma_l \cup \Gamma_u, \quad (40)$$

with  $\vartheta = \vartheta_{st} + \vartheta_{CH}$ . In fact, (40) is equivalent to  $\partial_n \vartheta = 0$  on  $\Gamma_l \cup \Gamma_u$ . Moreover, since (39) implies that the normal derivative of  $\vartheta_{CH}$  vanishes on  $\partial\Omega$ , it must also hold  $\partial_n \vartheta_{CH} = \nabla \vartheta_{CH} \cdot \mathbf{n} = 0$  on  $\Gamma_l \cup \Gamma_u$ , and Equation (40) thus leads to

$$\begin{aligned} \mathbf{J}_M \cdot \mathbf{n} &= -\frac{L_{MM}}{T} \nabla \vartheta_{st} \cdot \mathbf{n} = -\frac{L_{MM}}{T} \frac{\partial \vartheta_{st}}{\partial c} \nabla c \cdot \mathbf{n} = 0 \\ \Rightarrow \quad \nabla c \cdot \mathbf{n} &= 0, \quad \text{on } \Gamma_l \cup \Gamma_u. \end{aligned} \quad (41)$$

We conclude that the boundary conditions (38c) and (39) are equivalent to requiring the vanishing of the normal derivatives of the chemical potential and of the mass fraction (i.e., the so-called “wetting angle condition”) on  $\Gamma_l \cup \Gamma_u$ , as is usually the case in the numerical treatment of the Cahn-Hilliard model.

Looking at the boundary  $\Gamma_c \cup \Gamma_h$ , we notice that, by expressing  $\mathbf{J}_M$  as in (34) and invoking (39), the boundary condition (38c) becomes a homogeneous Robin-like condition on  $c$ . In fact, enforcing (39) allows to retrieve the zero-flux boundary condition of standard thermodiffusion (Benano-Melly et al., 2001), i.e.,

$$\mathbf{J}_M \cdot \mathbf{n} = -(\varrho_f D [\nabla c + (S_{st} + S_{CH})c(1-c)\nabla T]) \cdot \mathbf{n} = 0, \quad \text{on } \Gamma_c \cup \Gamma_h, \quad (42)$$

which could be considered as a “generalised wetting angle condition”. It is important to emphasise that, in the case of (42), the “wetting angle condition” is understood in a generalised way, i.e., it does *not* reduce to  $\partial_n c = \nabla c \cdot \mathbf{n} = 0$ , as in (41). Rather, (42) places the restriction that  $\partial_n c$  and  $\partial_n T$  balance each other according to the equation

$$\partial_n c + (S_{st} + S_{CH})c(1-c)\partial_n T = 0, \quad \text{on } \Gamma_c \cup \Gamma_h. \quad (43)$$

We remark that the condition  $\partial_n c = 0$  would be unphysical on  $\Gamma_c \cup \Gamma_h$ , since it would

necessarily imply the wrong result  $\partial_n T = 0$  on  $\Gamma_c \cup \Gamma_h$  (there is, indeed, no reason why the normal derivative of the temperature —and, thus, the normal heat flux, within our approximation— should vanish on this portion of the boundary). Note, also, that we speak of “Robin-like” boundary condition because Equation (42), or (43), is non-linear in  $c$  due to the term  $c(1 - c)$ . A Robin condition, instead, consists of a linear combination of a function and its derivative, restricted over a subset of the boundary of a computational domain.

## 4.2 Numerics

Equations (35a)–(35d) are implemented in a Finite Element software and have thus to be written in weak form. The procedure followed to obtain the weak form of (35a) and (35d) is standard, and will not be repeated here. Rather, we shall briefly sketch the main steps towards the weak formulation of (35b) and (35c). Since the mass fraction  $c$  is subjected to the Robin condition (38c), and its derivatives up to the fourth order are involved in the strong form of the problem, we choose the test function associated with the mass fraction as  $\tilde{c} \in H^2(\Omega)$ . Moreover, since  $\vartheta_{\text{CH}}$  has to comply with the Neumann condition (39), and its derivatives up to the second order feature in (35a)–(35d), we take  $\tilde{\vartheta} \in H^1(\Omega)$  as test function associated with  $\vartheta_{\text{CH}}$  (Salsa, 2008). Here,  $H^k(\Omega)$ , with  $k = 1, 2$ , denotes the Sobolev space  $H^k(\Omega) = \{u \in L^2(\Omega) : D^\alpha u \in L^2(\Omega)\}$ , where  $D^\alpha u = \frac{\partial^{|\alpha|} u}{\partial x_1^{\alpha_1} \dots \partial x_d^{\alpha_d}}$  is the distributional derivative of  $u$  of order  $\alpha$ , and  $\alpha = (\alpha_1, \dots, \alpha_d) \in \mathbb{N}^d$  is an arbitrary  $d$ -dimensional multi-index of length equal to, or smaller than,  $k$ , i.e.,  $|\alpha| = \alpha_1 + \dots + \alpha_d \leq k$  (Brezis, 1986).

By multiplying (35b) by  $\tilde{\vartheta}$ , and (35c) by  $\tilde{c}$ , integrating over  $\Omega$ , invoking Gauss’ The-



482 orem, and enforcing the boundary conditions (38d) and (39), we obtain

$$\int_{\Omega} \tilde{\vartheta} [\phi \varrho_0 \dot{c}] dV = - \int_{\Omega} \nabla \tilde{\vartheta} \cdot [\varrho_0 D \nabla c] dV \quad (44a)$$

$$\begin{aligned} & - \int_{\Omega} \nabla \tilde{\vartheta} \cdot [\varrho_0 D (S_{\text{st}} + S_{\text{CH}}) c (1 - c) \nabla T] dV \\ & - \int_{\Omega} \nabla \tilde{\vartheta} \cdot \left[ \frac{\varrho_0 D}{\partial \hat{\vartheta}_{\text{st}} / \partial c} \nabla \vartheta_{\text{CH}} \right] dV, \\ \int_{\Omega} [\tilde{c} \vartheta_{\text{CH}} - \nabla \tilde{c} \cdot (\lambda \nabla c)] dV &= \int_{\Gamma_c \cup \Gamma_h} \tilde{c} [\lambda (S_{\text{st}} + S_{\text{CH}}) c (1 - c) \partial_n T] dA. \end{aligned} \quad (44b)$$

483 To determine the finite element formulation of (44a) and (44b), we cover the computa-  
484 tional domain  $\Omega$  with a conforming, regular mesh  $\mathcal{T}_h$  consisting of  $N_h$  non-overlapping  
485 triangular elements  $\{K_i\}_{i=1}^{N_h}$ , and we introduce the finite dimensional spaces

$$\mathcal{V}_h^{(m)} = \{ \tilde{c}_h \in H^2(\Omega) : \tilde{c}_h|_{K_i} \in \mathbb{P}_m, \text{ for } i = 1, \dots, N_h \}, \quad (45a)$$

$$\mathcal{V}_h^{(n)} = \{ \tilde{\vartheta}_h \in H^1(\Omega) : \tilde{\vartheta}_h|_{K_i} \in \mathbb{P}_n, \text{ for } i = 1, \dots, N_h \}, \quad (45b)$$

486 where  $\mathbb{P}_m$  and  $\mathbb{P}_n$  are the set of polynomials of order  $m$  and  $n$ , respectively. The simulations  
487 reported in this paper were conducted with  $m = 2$  and  $n = 1$ . For completeness, we  
488 mention that polynomials of order 3 and 1 have been employed for discretising the test  
489 functions associated with pressure and temperature, respectively. In our simulations, the  
490 maximum element size is taken to be  $\max_{i=1}^{N_h} \ell_i \approx 2.5 \cdot 10^{-4}$  m, where  $\ell_i$  is the characteristic  
491 length of the  $i$ th finite element  $K_i$ .

492 To avoid the possibility of obtaining numerical variations in the results of the same  
493 order of magnitude as the truncation error, the mass fraction,  $c$ , has been rescaled as  
494  $c = c_0 \bar{c}$ , with  $c_0$  and  $\bar{c}$  being the initial and the “normalised” mass fraction, respectively.  
495 This is done, in particular, because of the very low reference mass fraction in the HDO-  
496 H<sub>2</sub>O mixture (see Table 1). Consequently, the mass balance law of the constituent  $\mathcal{C}_1$  is  
497 transformed into

$$\phi \varrho_0 \dot{\bar{c}} = \text{div} \left[ \varrho_0 D \left( \nabla \bar{c} + (S_{\text{st}} + S_{\text{CH}}) \bar{c} (1 - c_0 \bar{c}) \nabla T + \frac{1}{\partial \hat{\vartheta}_{\text{st}} / \partial \bar{c}} \nabla \vartheta_{\text{CH}} \right) \right]. \quad (46)$$

Our numerical solutions are normalised in such a way that the rescaled initial mass fraction in the computational domain is unitary for both the considered benchmarks, since  $c_0 = c(x, 0)$  is the “true” initial mass fraction of  $\mathcal{C}_1$ . All the quantities introduced in the model are coherently rescaled.

The weak form of the system of equations (35a)–(35d) has been spatially solved by means of Newton’s method, and the time discretisation has been performed adaptively by means of a Backward Differentiation Formula (BDF).

### 4.3 Model Parameters

The first experiment here studied considers a mixture of water ( $\text{H}_2\text{O}$ ) and heavy water (HDO). Benano-Melly et al. (2001) assumed that the mass fraction of heavy water, identified with the constituent  $\mathcal{C}_1$  of the mixture, and playing the role of the solute, is so small that the term  $(1 - c)c$  in (34) can be approximated as  $(1 - c)c \approx c$ . In our simulations, however, we kept the nonlinear term  $(1 - c)c$ , even when it was quite small, for the sake of generality. In addition to the boundary conditions (38a)–(38d) and (39), we impose that the initial mass fraction is uniformly distributed within the thermogravitational cell, and given by  $c_0 = 5.8 \cdot 10^{-6}$ . The value attributed to  $c_0$  has been obtained from the work by Jamet et al. (1992), in which the initial distribution of the solute was expressed in molarity and taken equal to  $C_0 = 2.9 \cdot 10^{-4}$  mol/l. The mass density of the mixture is expressed constitutively by the formula (Benano-Melly et al., 2001)

$$\varrho_f = \hat{\varrho}_f(c, T) = \varrho_0 [1 - \beta(T - T_{\text{ref}}) + \gamma(c - c_{\text{ref}})], \quad (47)$$

where  $\beta$  and  $\gamma$  are the (constant) thermal and solutal expansion coefficients of the fluid, respectively, and  $T_{\text{ref}}$  and  $c_{\text{ref}}$  are reference values of the temperature and solutal mass fraction. In particular, the dependence of  $\hat{\varrho}_f$  on  $c$  is neglected in (47) (i.e.,  $\gamma$  is set equal to zero), because the difference between the mass density of heavy water and the mass density of the mixture as a whole is very small (incidentally, this also implies that no reference value of the mass fraction,  $c_{\text{ref}}$ , needs to be prescribed). Thus, the mass density

actually used in the numerical simulations is  $\hat{\varrho}_f(T) = \varrho_0 [1 - \beta(T - T_{\text{ref}})]$ . Moreover, the viscosity of the mixture is assumed to be constant.

The second experiment considers a mixture of tetracosane-dodecane,  $\text{C}_{24}\text{H}_{50}$ - $\text{C}_{12}\text{H}_{26}$ . The constituent  $\mathcal{C}_1$ , identified with the tetracosane,  $\text{C}_{24}\text{H}_{50}$ , is assumed to have uniform initial mass fraction  $c_0 = 0.15$ , a value much higher than that assigned in the first experiment. This higher concentration is expected to lead to a stronger contribution of both the standard and the non-standard thermodiffusion effects. While the viscosity of the mixture as a whole is regarded as a constant also in this experiment, the mass density  $\varrho_f$  is prescribed by the empirical formula [slightly adapted from Jamet et al. (1992)]

$$\varrho_f = \hat{\varrho}_f(c; x) = \frac{758.30 \cdot (1 - 5.712 x)}{1 - 758.30 \cdot (1 - 5.712 x) \cdot 8 \cdot 10^{-5} c}, \quad (48)$$

where  $x \in [0, H]$  is the space coordinate along the direction of the width of the thermogravitational cell.

The parameters employed for simulating both these experiments are listed in Table 1. In particular,  $\Delta T \equiv T_h - T_c$  represents the temperature difference between the hot side,  $\Gamma_h$ , and the cold side,  $\Gamma_c$ , of the computational domain,  $\Omega$ , while the reference temperature  $T_{\text{ref}}$  is defined as the arithmetical mean between  $T_c$  and  $T_h$ , i.e.,  $T_{\text{ref}} \equiv (T_c + T_h)/2$ . By reading off  $T_{\text{ref}}$  and  $\Delta T$  from Table 1, we obtain  $T_c = 309.15$  K,  $T_h = 334.15$  K. It is also worthwhile to remark that the initial value of the tetracosane mass fraction,  $c_0$ , has been computed by using the experimental values reported in Table 2:  $c_0 = \frac{\chi_1}{\chi_1 + \chi_2} \approx 0.15$ , while the reference mass density of the mixture,  $\varrho_0$ , has been taken equal to  $\varrho_0 = 758.30$  kg/m<sup>3</sup>. Note that this value is close enough to the value of the density that would be computed according to the assumption of ideal mixture (Oldenburg and Pruess, 1998):  $\varrho_0 = \left( \frac{c_0}{\varrho_1} + \frac{1-c_0}{\varrho_2} \right)^{-1} \approx 757.93$  kg/m<sup>3</sup>, where the true densities  $\varrho_1$  and  $\varrho_2$  refer to the densities of the “pure” constituents  $\text{C}_{24}\text{H}_{50}$  and  $\text{C}_{12}\text{H}_{26}$ .

The modelling choice (48), done to comply with Jamet et al. (1992), requires some words of explanation. Indeed, as in (47), the equation of state for the fluid mass density should express  $\varrho_f$  as a function of the state variables that are regarded as independent, i.e., temperature,  $T$ , and solutal concentration,  $C$ , in the approach followed in this work.

In particular, by slightly adapting Equation (15) of Jamet et al. (1992) to our framework and notation, we prescribe

$$\varrho_f = \tilde{\varrho}_f(C, T) = \varrho_0 \{1 - \beta[T - T_c]\} \{1 + \alpha_c C\}, \quad \Rightarrow \quad (49a)$$

$$\varrho_f = \hat{\varrho}_f(c, T) = \frac{\varrho_0 \{1 - \beta[T - T_c]\}}{1 - \varrho_0 \{1 - \beta[T - T_c]\} \alpha_c c}, \quad (49b)$$

where  $c = C/\varrho_f$  is the solutal mass fraction, and  $T_c$  is the temperature imposed by means of the Dirichlet boundary condition  $T|_{\Gamma_c} = T_c$  on the cold boundary,  $\Gamma_c \subset \partial\Omega$ . To obtain (48) from (49b), we proceed in two steps: First, we set  $\alpha_c = 8 \cdot 10^{-5}$  and  $\varrho_0 = 758.30 \text{ kg/m}^3$  (note that Jamet et al. (1992) use the value  $741.1 \text{ kg/m}^3$  in lieu of  $758.30 \text{ kg/m}^3$ ). Then, upon using Equation (15) of Jamet et al. (1992), we write

$$1 - \beta[T - T_c] = 1 + \alpha_x x, \quad (50)$$

which, evaluated at  $x = H$ , yields  $T_h - T_c = \Delta T = -(\alpha_x H)/\beta$ , and  $\beta = -(\alpha_x H)/\Delta T$ . This result can be used to estimate the thermal expansion coefficient,  $\beta$ . Indeed, setting  $\alpha_x = -5.712 \text{ m}^{-1}$  (Jamet et al., 1992) leads to  $\beta \approx 10^{-3} \text{ K}^{-1}$ , a value of the same order of magnitude as those prescribed by Jamet et al. (1992) for  $\text{C}_{24}\text{H}_{50}$  and  $\text{C}_{12}\text{H}_{26}$ , i.e.,  $\beta_{\text{Jamet}}^{\text{C}_{24}\text{H}_{50}} = 8.1 \cdot 10^{-4} \text{ K}^{-1}$  and  $\beta_{\text{Jamet}}^{\text{C}_{12}\text{H}_{26}} = 9.6 \cdot 10^{-4} \text{ K}^{-1}$ , respectively.

We emphasise that (50) amounts to *impose*, rather than to compute, the temperature distribution in the thermogravitational cell, and to identify it with

$$T \equiv T(x) = T_c - \frac{\alpha_x H}{\beta} \frac{x}{H} = T_c + \Delta T \frac{x}{H}. \quad (51)$$

Although this result complies with the conditions  $\nabla T \cdot \mathbf{n} = 0$  on  $\Gamma_1 \cup \Gamma_u$  as well as  $T|_{\Gamma_c} = T_c$  and  $T|_{\Gamma_h} = T_h$ , Equation (51) is, in fact, the solution of  $\text{div}(\kappa \nabla T) = \kappa \partial^2 T / \partial x^2 = 0$ , which is obtained from (35d) in the stationary limit, and by neglecting the terms  $\text{div}(\varrho_0 C_{\text{pf}} T \mathbf{w})$  and  $\phi \varrho_0 \vartheta_{\text{CH}} \dot{c}$ . In this work, this approximation is employed only for the simulation of the mixture  $\text{C}_{24}\text{H}_{50}$ - $\text{C}_{12}\text{H}_{26}$ .

## 5 Results

In this section, we validate our model by recomputing the numerical experiments discussed by Jamet et al. (1992) and Benano-Melly et al. (2001), and we show how the introduction of the term  $\frac{1}{2}\lambda\|\nabla c\|^2$  into the Helmholtz free energy density of the fluid phase (in fact, a mixture of two fluid constituents) produces a small, yet visible, correction to the results obtained within the setting of standard thermodiffusion. This correction manifests itself in (34) through the Cahn-Hilliard Soret coefficient,  $S_{\text{CH}}$ , and the term proportional to  $\nabla\vartheta_{\text{CH}}$ , and has repercussions on the evolution of the solute (i.e., the constituent  $\mathcal{C}_1$ ).

### 5.1 Validation of the model

It has been shown in some works (cf. e.g. Benano-Melly et al. (2001); Fargue et al. (1998); Jamet et al. (1992); Rowley and Horne (1980)) that, if an initially uniform fluid mixture saturating a porous medium is exposed to a thermal gradient, and is subjected to the buoyancy effect due to gravity, a separation of the mixture's constituents will be initiated. The degree of separation depends on the properties of the constituents and on permeability of the porous medium. A typical behaviour that can be registered in a thermogravitational cell, while the mixture evolves in time, is reported in Figure 1a.

Benano-Melly et al. (2001) pointed out that, depending on the sign of the Soret coefficient, at the steady state the heaviest constituent of the mixture finds itself at the bottom of the cell, close to the cold side. The distortion of the mass fraction isolines shown in Figure 1a is the outcome of the motion induced by the coupling between gravity and the horizontal thermal gradient. The interaction between these two entities characterises the results of the thermogravitational cell experiment. Consistently with expectations, in our simulations the steady state is approached in a characteristic time that depends on the considered mixture. After the formation of an initial horizontal gradient of mass fraction, so that the mass fraction isolines are all parallel to the vertical symmetry axis of the cell, the evolution of the system towards the steady state is characterised by a distortion and rotation of the isolines, whose consequence is the redistribution of the

fluid mixture with the heaviest constituent at the bottom. Figure 1a has been produced for comparison with similar results previously obtained by Benano-Melly et al. (2001) and Fargue et al. (1998).

The quantity introduced to measure the degree of separation achievable in the mixture occupying a thermogravitational cell is the *separation ratio* (Benano-Melly et al., 2001)

$$b_{\infty} \equiv \frac{c_{B\infty}/(1 - c_{B\infty})}{c_{T\infty}/(1 - c_{T\infty})}, \quad (52)$$

where  $c_{B\infty}$  and  $c_{T\infty}$  denote, respectively, the mass fractions of the solute reached, at the stationary state, at the bottom and at the top of the thermogravitational cell. The separation ratio,  $b_{\infty}$ , depends on the geometry of the cell, on the applied thermal gradient, and on the material properties of both the fluid mixture and the porous medium filling the cell. For instance, in the case of an isotropic porous medium (so that its permeability tensor is spherical, i.e.,  $\mathbf{k} = k\mathbf{I}$ , and entirely represented by the scalar permeability  $k$ ), and for a prescribed set of model parameters, the separation ratio can be expressed as a function of the scalar permeability. In particular, it is possible to determine an optimal value of  $k$ , denoted by  $k_{\star}$  hereafter, such that  $b$  is maximum. Benano-Melly et al. (2001) supply an approximated formula relating the maximum separation ratio,  $b_{\infty}^{\max}$ , with the assigned parameters, i.e.,

$$\log(b_{\infty}^{\max}) = \frac{S_{\text{st}}\Delta TL\sqrt{120}}{24H}. \quad (53)$$

According to (53), for a given thermal gradient,  $\Delta T/H$ , and cell height,  $L$ , the maximum separation ratio achievable in the cell can be determined once  $S_{\text{st}}$  is known, and vice versa. More details on this topic can be found in the works by Lorenz and Emery (1959), and Emery and Lorenz (1963).

In studying the separation of heavy water, HDO, in the HDO-H<sub>2</sub>O mixture, Benano-Melly et al. (2001) observed a discrepancy between the experimental results and the analytical and numerical predictions of the separation ratio and the steady state. A similar discrepancy was also observed by Jamet et al. (1992) also for the C<sub>24</sub>H<sub>50</sub>-C<sub>12</sub>H<sub>26</sub> mixture. To the best of our understanding, both Benano-Melly et al. (2001) and Jamet

et al. (1992) conducted their investigations within the standard setting of thermodiffusion, and determined suitable transport and flow properties in order to obtain a good fitting of the experimental data. In particular, Benano-Melly et al. (2001) considered dispersion in the solutal mass flux vector, Jamet et al. (1992) assumed that the porous matrix was transversely isotropic with respect to the permeability, and Fargue et al. (1998) studied the influence of a variable dispersive effect on the reduction of the discrepancy between the numerical and the experimental results.

To validate the model presented in this paper, we start by showing that our numerical simulations are able to reproduce the same trend as that of the curves obtained by Jamet et al. (1992). To this end, we first consider standard thermodiffusion, which amounts to set  $\lambda = 0 \text{ m}^4/\text{s}^2$  in (9) and, consequently, to switch off all the terms of the model featuring the subscript “CH”. The outputs of our numerical simulations are reported in Figure 2, in which the separation ratio for both the HDO-H<sub>2</sub>O and the H<sub>24</sub>C<sub>50</sub>-H<sub>12</sub>C<sub>26</sub> mixture is plotted as a function of the permeability of the porous medium. The parameters used for these numerical simulations are specified in Tables 1 and 2. The value of the Soret coefficient,  $S_{\text{st}}$ , has been taken from Benano-Melly et al. (2001) and Fargue et al. (1998) for the HDO-H<sub>2</sub>O mixture, and from Jamet et al. (1992) for the H<sub>24</sub>C<sub>50</sub>-H<sub>12</sub>C<sub>26</sub> mixture.

Although our results are in agreement with both the analytical and the numerical curves obtained by Jamet et al. (1992), and in spite of the fact that all these curves seem to reproduce qualitatively the arrangement of the experimental points, none of them meets quantitatively the experimental data. To do so, the numerical and analytical curves should be shifted to the right. It is also worthwhile to emphasise that the maximum separation ratio, as predicted by both the analytical and the numerical computations, is close to the one determined experimentally, but it corresponds to a value of permeability that is quite smaller than the experimental one. For example, with the choice of parameters supplied in Tables 1 and 2, and for the HDO-H<sub>2</sub>O mixture, the maximum separation ratio is  $b_{\infty}^{\text{max}} = 1.0563$ . Nevertheless, this value is obtained for a permeability different from the experimental one, which is instead approximatively given by  $k \approx 1.0 \cdot 10^{-10} \text{ m}^2$ . We recall here that the analytical curves in Figure 2 were obtained by Lorenz and Emery (1959)

and Emery and Lorenz (1963).

## 5.2 Influence of the Cahn-Hilliard terms

According to Fargue et al. (1998), while the growth of the separation ratio is related to the augmentation of  $S_{\text{st}}$ , the offset to the right of the bell-like curves in Figures 2a and 2b is primarily due to the increase of the coefficient  $D$  in the mass flux vector  $\mathbf{J}_M$ . Within the standard setting of thermodiffusion, this may occur either for higher solutal and thermal diffusion coefficients or in response to dispersion, which adds itself to diffusion, thereby contributing to increment  $D$ . Beside these behaviours, in our work we also observed that, if the factor  $\lambda$  is switched on in (9), the increase of  $\lambda$  produces both an increase of the separation ratio and an offset of the bell-like curves to the right. We remark that switching on  $\lambda$  means to activate the Cahn-Hilliard chemical potential  $\vartheta_{\text{CH}}$ , its gradient, and the additional Soret coefficient  $S_{\text{CH}}$ , which all contribute to the mass flux vector in a non-trivial way. In particular, in our simulations we observed that the shift of the curves depicted in Figure 3a can be attributed to the last summand on the right-hand-side of (34), which is proportional to  $\nabla\vartheta_{\text{CH}}$ , and describes a transport of mass that can be interpreted as a “second-order diffusion”. Indeed, the term  $\nabla\vartheta_{\text{CH}}$  involves the third-order derivatives of the mass fraction. The contribution associated with  $\nabla\vartheta_{\text{CH}}$  is principally active at the top and at the bottom of the thermogravitational cell, and is otherwise irrelevant unless the mass fraction is distributed in a sufficiently non-uniform way. Looking at Figure 3a, we notice that the strength of the non-standard thermodiffusive effects depends also on the permeability. Indeed, for permeabilities sufficiently smaller than  $k_*$ , the separation ratios obtained for different values of  $\lambda$  lie closer to each other than those obtained for  $k \approx k_*$ . Moreover, also the initial mass fraction of the solute is a key parameter that can affect the weight of the terms triggering the non-standard thermodiffusion.

To estimate the influence of the non-standard terms generated by nonzero values of  $\lambda$ , we compute  $\varepsilon = 100 \left[ \frac{\max_{\Omega} |c_{\text{st}} - c_{\lambda}|}{\max_{\Omega} c_{\text{st}}} \right]$ , where  $c_{\text{st}}$  is the mass fraction determined within the standard setting of thermodiffusion, i.e., for  $\lambda = 0$ , and  $c_{\lambda}$  is the mass fraction calculated for nonzero values of  $\lambda$ . The evolution of  $\varepsilon$  in time and its relation with the permeability



of the porous medium are shown in Figures 3b and 3c for the HDO-H<sub>2</sub>O mixture. The discrepancies shown in Figure 3a are consistent with the curves plotted in Figure 3c, where  $\varepsilon$  becomes noticeable only for permeabilities close to  $k_\star \in [1, 3] \cdot 10^{-11} \text{ m}^2$ . From Figure 3b, one can observe that the effect of  $\lambda$  manifests itself also in the asymptotic value of  $\varepsilon$ , which characterises the stationary conditions of the system.

It should be mentioned that, in order for the Cahn-Hilliard chemical potential,  $\vartheta_{\text{CH}}$ , to give non-negligible contributions to thermodiffusion, it is necessary to build a non-null gradient of mass fraction inside the thermogravitational cell. When the mass fraction  $c$  is initially uniform in the cell, and  $S_{\text{st}}$  is set equal to zero *a priori*, the terms  $S_{\text{CH}}$  and  $\nabla \vartheta_{\text{CH}}$  are unable to generate a mass flux and, consequently, no separation can be observed, regardless of the magnitude of the imposed thermal gradient. Conversely, if a nontrivial pattern of mass fraction is present (e.g. in the experiment studied by Rowley and Horne (1980)), the contributions to the mass flux stemming from  $S_{\text{CH}}$  and  $\nabla \vartheta_{\text{CH}}$  are visible, even without the presence of the standard Soret coefficient. Such evidence is highlighted in Figure 4a, where the transient evolution in time of the mass fraction at the top,  $c_{\text{T}}$ , and at the bottom,  $c_{\text{B}}$ , is reported. To obtain the results in Figure 4a, we imposed a non-uniform initial distribution of solute in the domain (see Figure 4b). The non-uniform mass fraction used as initial condition for this numerical experiment is “prepared” by taking the stationary distribution of C<sub>24</sub>H<sub>50</sub> obtained by solving (35a)–(35d) with  $S_{\text{st}} = 1.2 \cdot 10^{-4} \text{ 1/K}$  and  $\lambda = 3.8 \text{ m}^4/\text{s}^2$ . Recalling the expression of the effective Soret coefficient,  $S_{\text{eff}} = S_{\text{st}} + S_{\text{CH}}$ , the lines with no markers correspond to  $S_{\text{eff}} = 0$ , the lines with circles to  $S_{\text{eff}} = S_{\text{CH}}$ , and the lines with asterisks to  $S_{\text{eff}} = S_{\text{st}}$ . This is done to visualise the effect of  $S_{\text{CH}}$  and  $S_{\text{st}}$  on the mass fraction. When  $S_{\text{eff}} = 0$ , and the mass flux vector reduces to  $\mathbf{J}_{\text{M}} = -\rho_{\text{f}} D \nabla c$ , the mass fractions at the top and the bottom of the cell tend towards a common value, thereby making the mixture uniform at the steady state. Also in the second case, i.e., when  $S_{\text{eff}} = S_{\text{CH}}$ , the mass fractions  $c_{\text{B}}$  and  $c_{\text{T}}$  converge to the same common value as in the first case. However, the time required to approach the steady state is more than six times longer than the one needed when  $S_{\text{eff}} = 0$ . Finally, when  $S_{\text{eff}} = S_{\text{st}}$ , the mass fractions  $c_{\text{B}}$  and  $c_{\text{T}}$  approach stationary values

over a characteristic time comparable with that of the first case, but these values are different from one another, i.e.,  $c_{B\infty} \neq c_{T\infty}$ , thereby allowing for a nontrivial separation ratio. Starting with an initial separation ratio  $b_0 = 2.3407$ , we obtain  $b_\infty = 1.0384$ . We recall that the initial value of the separation ratio is linked to a simulation in which  $S_{\text{eff}} = S_{\text{st}} + S_{\text{CH}}$ , i.e., it is the value of  $b$  obtained with the same  $S_{\text{st}}$ , but also with the Cahn-Hilliard contribution. This value of  $b$ , then, is clearly amplified of about 40% by the presence of the Cahn-Hilliard effect. The corresponding curve is reported in Figure 2d.

### 5.3 Main results

This section is dedicated to the main results of our study, i.e., the description of the role played by  $S_{\text{CH}}$  on the curves expressing the separation ratio versus the permeability, and the determination of a relation between the effective Soret coefficient  $S_{\text{eff}} = S_{\text{st}} + S_{\text{CH}}$  and the permeability.

Looking at Figure 2c, one can see that our separation ratios are in good agreement with those obtained by Fargue et al. (1998), and fit the experimental data quite satisfactorily for  $\lambda = 2.7 \cdot 10^4$  1/K and  $S_{\text{st}} = 1.0 \cdot 10^{-5}$  1/K. We emphasise that, while we determined our results by introducing the Cahn-Hilliard correction to standard thermodiffusion, Fargue et al. (1998) considered different values of the dispersion coefficient, which correspond to the dashed blue curve and to the red curve marked with circles. Although  $\lambda$  is quite big in this example, the value of  $S_{\text{st}} = 1.0 \cdot 10^{-5}$  1/K is the same as that taken by Fargue et al. (1998) (and a little bit smaller than that in Table 1). It is useful to mention that the Soret coefficient  $S_{\text{st}} = 1.0 \cdot 10^{-5}$  1/K would not allow to reach the congruence actually achieved with the separation ratios determined experimentally if neither  $S_{\text{CH}}$  nor any other contribution to the mass flux vector (as, for instance, dispersion) were taken into account. Indeed, the curve corresponding to  $S_{\text{st}} = 1.0 \cdot 10^{-5}$  1/K and  $\lambda = 0$ , i.e., the solid line in Figure 2c, is far away from the experimental predictions.

The results regarding the  $\text{C}_{24}\text{H}_{50}$ - $\text{C}_{12}\text{H}_{26}$  mixture are reported in Figure 2d. Different choices of the pair  $(S_{\text{st}}, \lambda)$  are made to fit the experimental data. However, only for  $S_{\text{st}} = 1.2 \cdot 10^{-4}$  1/K and  $\lambda = 3.8$  m<sup>4</sup>/s<sup>2</sup> the experimental points corresponding to high

permeabilities are fitted satisfactorily. The uncertainty in the selection of the appropriate pair  $(S_{\text{st}}, \lambda)$  could be due to a lack of information about the considered mixture, and a possible misreading of the numerical points, for which the precise position of the optimum value of  $k$  could be less plausible (Fargue et al., 1998). Moreover, in the related simulations, the fluid viscosity  $\mu$ , although evaluated with the formula reported in Jamet et al. (1992), is here taken as a constant, namely  $\mu = \hat{\mu}(c_0)$ .

Finally, in Table 3, we reported the maximum and minimum  $S_{\text{eff}}$  for each of the curves shown in Figure 2d. Indeed, as previously noticed, while  $S_{\text{st}}$  is a constant value, as prescribed by the literature,  $S_{\text{CH}}$  can vary within the domain according to the sign of  $\nabla c$ .

From Table 3 we see that both  $S_{\text{eff,max}}$  and  $S_{\text{eff,min}}$  diminish with diminishing  $S_{\text{st}}$ , but the discrepancy between  $S_{\text{st}}$  and  $S_{\text{CH}}$  increases with increasing  $\lambda$ , even though  $S_{\text{st}}$  is lower when a higher value of  $\lambda$  is considered. This happens to balance the value of  $S_{\text{eff}}$ , which is ruled by the sum of  $S_{\text{st}}$  and  $S_{\text{CH}}$ . We remark that the value of  $S_{\text{eff}}$  can also be smaller than  $S_{\text{st}}$ , since  $S_{\text{CH}}$  may be negative. To give an idea of these occurrences, we refer to Figure 1b and Figure 1c. In these figures, the ends of the computational domain have been zoomed, since the actual width of the cell is too thin. Figure 1b refers to a small value of  $k$ , whereas Figure 1c refers to a higher value of  $k$ . The normalised isolines of the mass fraction at the steady state are shown in the first column of each of these two figures. In these columns, the blue isolines represent smaller values of  $S_{\text{CH}}$ , whereas the red isolines are for higher values. One can see that  $S_{\text{CH}}$  diminishes at the hot and at the bottom boundaries of the cell, where it also attains negative values, and increases at the cold and top boundaries of the cell. In the case of low permeability (see the second and third column of Figures 1b), the mass fraction isolines are arranged almost linearly in the domain, so that the majority of the solute is at the bottom left corner of the cell. Thus, in this case, the arrangement of the solute is preferentially at the bottom. The corresponding  $S_{\text{CH}}$  is then negative at the bottom and at the cold side, and positive at the top. For higher permeabilities, the mass fraction isolines feature a rather curvy pattern (Figure 1c). Also in this case, the heaviest constituent in the mixture evolves in

such a way that it is more concentrated at the bottom of the cell. However, the Cahn-Hilliard Soret coefficient,  $S_{\text{CH}}$ , is now distributed variably from the left to the right. The negative values of  $S_{\text{CH}}$  can be found at the hot side and the positive ones at the cold side, whereas at the bottom and at the top ends both positive and negative values can be observed. We recall that  $S_{\text{CH}}$  depends on the Laplacian of the mass fraction through  $\vartheta_{\text{CH}}$ , which, in the case under study, is positive at the cold side. Therefore, at a given instant of time, the maximum and the minimum of  $S_{\text{eff}}$  are attained in the domain. The mean value of the effective Soret coefficient is approximatively in the middle of the domain at each height. The sign of this coefficient is then ruled by the sign of the second gradient of the mass fraction itself, since  $S_{\text{CH}}$  depends on the non-standard chemical potential, as defined in (33).

A remarkable difference between the two considered experiments analysed in this paper is the choice of  $\lambda$ . Although we determined  $\lambda$  by having recourse to the Cahn number (Lowengrub and Truskinovsky, 1998), the way in which this number is defined may necessitate revisions. In particular, the choice of the characteristic mesoscale, and the characteristic coarse scale could lead to quite big variations of the Cahn number. Moreover, if the solute mass fraction is low in the domain, then a higher  $\lambda$  is required to make the Cahn-Hilliard contribution weighty. This is the case of the mixture HDO-H<sub>2</sub>O, for which the optimal  $\lambda$  is  $\lambda = 2.7 \cdot 10^4 \text{ m}^4/\text{s}^2$ . Vice versa, for the mixture C<sub>24</sub>H<sub>50</sub>-C<sub>12</sub>H<sub>26</sub>, the solute mass fraction is three orders of magnitude higher, thereby producing a required  $\lambda$  that is in the neighbourhood of unity.

## 6 Conclusions and outlook

In this work, we studied the evolution of the composition of a two-constituent fluid mixture flowing through a porous medium exposed to a non-uniform thermal field. The mixture's composition was described by the mass fraction of one constituent, denoted by  $\mathcal{C}_1$ . In accordance with the standard theory of Thermodiffusion, the thermal gradient developed in the mixture,  $\nabla T$ , contributes to transport the mass of  $\mathcal{C}_1$  by inducing the term

$\mathbf{J}_{\text{MQ}}^{\text{st}} \equiv -\varrho_{\text{f}} D S_{\text{st}} c(1 - c) \nabla T$ , which augments the purely diffusive(-dispersive) Fick's mass flux vector associated with  $\mathcal{C}_1$ . The magnitude of the Soret coefficient,  $S_{\text{st}}$ , determines the thermodiffusive strength.

We proposed a generalisation of the standard framework of thermodiffusion based on the assumption that the Helmholtz free energy density of the fluid is of the Cahn-Hilliard type [cf. Equation (9)]. The main consequence of this hypothesis is that the mass flux vector acquires two additional quantities: The first quantity is proportional to  $\nabla \vartheta_{\text{CH}}$ , with  $\vartheta_{\text{CH}}$  being referred to as the Cahn-Hilliard chemical potential [cf. Equation (12b)], while the second one is given by  $-\varrho_{\text{f}} D S_{\text{CH}} c(1 - c) \nabla T$ , and is formally identical to  $\mathbf{J}_{\text{MQ}}^{\text{st}}$  except for the fact that  $S_{\text{st}}$  is replaced by the Cahn-Hilliard Soret coefficient  $S_{\text{CH}}$  [cf. Equation (33)].

We tested our model by solving two benchmark problems taken from the literature, and compared our results with those of other authors [cf. Figures 2a, 2b, 2c, and 2d]. In particular, we focused on the determination of the separation ratio attainable in a thermogravitational cell. Following Jamet et al. (1992), Fargue et al. (1998), and Benano-Melly et al. (2001), we simulated these experiments by considering the fluid mixtures HDO-H<sub>2</sub>O and C<sub>24</sub>H<sub>50</sub>-C<sub>12</sub>H<sub>26</sub>. Firstly, we observed that, since the Cahn-Hilliard contributions arise when the mass fraction varies in space, their strength increases with the separation ratio. Moreover, it is necessary to adapt the effective Soret coefficient  $S_{\text{eff}} = S_{\text{st}} + S_{\text{CH}}$  to obtain the required separation. Secondly, we noticed that the discrepancies between the analytical and the experimental values of the optimal permeability and the corresponding separation ratio could be imputed to dispersion, which affects the coefficient  $D$ , and to a lack of knowledge of all the parameters of the model. Still, for the mixture HDO-H<sub>2</sub>O, the introduction of  $S_{\text{CH}}$ , and the definition of the effective Soret coefficient  $S_{\text{eff}}$ , led to a good agreement with the experimental curves that express the separation ratio as a function of the permeability [cf. Figures 2c and 2d]. For the mixture C<sub>24</sub>H<sub>50</sub>-C<sub>12</sub>H<sub>26</sub>, instead, our best fit of the experimental data could only approximate the expected curve. This was due to quite a large amount of uncertainty of some experimental values used as model parameters [cf. also with Fargue et al. (1998)]. In addition, a stronger contribution of the

Cahn-Hilliard contributions was registered, also because the mass fraction of the solute is quite bigger than in the thermogravitational cell studied for the HDO-H<sub>2</sub>O experiment.

For future research it could be interesting to employ the theoretical framework outlined in this paper to the thermodiffusion in physical systems for which an initial gradient of mass fraction is present [cf., for example, Rowley and Horne (1980)]. Furthermore, also the contribution provided by the Korteweg stress tensor to Darcy’s law necessitates a more thorough study.

## Acknowledgments

This work has been supported in part by the *Politecnico di Torino* (Italy) and in part by the *Fondazione Cassa di Risparmio di Torino* (Italy), through the *La Ricerca dei Talenti* (“HR Excellence in Research”) programme. AG dedicates this work Prof. Gaetano Giaquinta (25th of November 1945 - 16th of August 2016). AG warmly thanks Mr. Salvatore Di Stefano and Dr. Ariel Ramírez-Torres for precious help.

## References

- Anderson, D.M. and McFadden, G.B., Diffuse-Interface Methods in Fluid Mechanics, *Annual Review of Fluid Mechanics*, vol. **30**, pp. 139–165, 1998.
- Bear, J. and Bachmat, Y., *Introduction to Modeling of Transport Phenomena in Porous Media*, Dordrecht, Boston, London: Kluwer, 1990.
- Benano-Melly, L.B., Caltagirone, J.-P., Faissat, B., Montel, F. and Costeséques, P., Modeling Soret coefficient measurement experiments in porous media considering thermal and solutal convection, *International Journal of Heat and Mass Transfer*, vol. **44**, pp. 1285–1297, 2001.
- Bennethum, L., Murad, M.A. and Cushman, J.H., Macroscale Thermodynamics and the chemical potential for swelling porous media, *Transport in Porous Media*, vol. **39**, pp. 187–225, 2000.

- Brezis, H., *Analisi Funzionale – Teoria e Applicazioni*, Napoli (Italy): Liguori Editore, pp. 248, 1986 (In Italian)
- Celestino, A., Leonardi, E. and Maciocco, L., A computational study of salt diffusion and heat extraction in solar pond plants, *Solar Energy*, vol. **80**, pp. 1498–1508, 2006.
- Chandra Shekar, B., Kishan, N. and Chamka, A.J., Soret and Dufour effects on MHD natural convective heat and solute transfer in a fluid-saturated porous cavity, *Journal of Porous Media*, vol. **19**, no. 8, pp. 669–686, 2016.
- Chavepeyer, G., Dutrieux, J.F., Van Vaerenbergh, S. and Legros, J.C., A Survey of the Thomaes Flow Cell Method for the Soret Coefficient, in *Thermal Nonequilibrium Phenomena in Fluid Mixtures*, W. Kohler and S. Wiegand, Eds.: Berlin, Heidelberg: Springer-Verlag, pp. 211–232, 2002.
- Chen, C.-Y. and Yan, P.-Y., A diffuse interface approach to injection driven flows of different miscibility in heterogeneous porous media, *Physics of Fluids*, vol. **27**, pp. 083101-1–083101-19, 2015.
- Chen, C.-Y. and Yan, P.-Y., Radial flows in heterogeneous porous media with linear injection scheme, *Computers & Fluids*, vol. **142**, pp. 30–36, 2017.
- Choi, Y.J. and Anderson, P.D., Cahn-Hilliard modeling of particles suspended in two-phase flows, *International J. of Num. Meth. in Fluids*, vol. **69**, no. 5, pp. 995–1015, 2012.
- Collins, C., Shen, J. and Wise, S.M., An efficient, energy stable scheme for the Cahn-Hilliard-Brinkman system, *Commun. Comput. Phys.*, vol. **13**, pp. 929–957, 2013.
- Costeséques, P., Fargue, D. and Jamet, P., Thermodiffusion in Porous Media and Its Consequences, in *Thermal Nonequilibrium Phenomena in Fluid Mixtures*, W. Köhler and S. Wiegand, Eds., Berlin, Heidelberg, New York: Springer-Verlag, pp. 389–427, 2002.

- 870 Cueto-Felgueroso, L. and Juanes, R., A phase field model of unsaturated flow, *Water*  
871 *Resources Research*, vol. **45**, pp. W10409-1–W10409-23, 2009.
- 872 Davarzani, H., Marcoux, M. and Quintard, M., Theoretical predictions of the effective  
873 thermodiffusion coefficients in porous media, *Int. J. Heat and Mass Transfer*, vol. **53**,  
874 pp. 1514–1528, 2010.
- 875 Davarzani, H. and Marcoux, M., Influence of solid phase thermal conductivity on species  
876 separation rate in packed thermogravitational columns: A direct numerical simulation  
877 model, *Comptes Rendus Mechanique*, vol. **339**, no. 5, pp. 355–361, 2011.
- 878 Davis, H.T., A theory of tension at a miscible displacement front, in *Proceedings of the*  
879 *Symposium on Numerical Simulation in Oil Recovery*, M.F. Wheeler, Ed., New York,  
880 NY, USA: Springer-Verlag, pp. 105–110, 1988.
- 881 De Groot S.R. and Mazur P., *Non-Equilibrium Thermodynamics*, Mineola, USA: Dover  
882 Publications, Inc., 1984.
- 883 Dias, E.O. and Miranda, J., Control of radial fingering patterns: a weakly nonlinear  
884 approach, *Phys. Rev. E*, vol. **81**, no. 1, pp. 016312-1–016312-7, 2010.
- 885 Diegel, A.E., Feng, X.H. and Wise, S.M., Analysis of a Mixed Finite Element Method for  
886 a Cahn-Hilliard-Darcy-Stokes system, *SIAM Journal of Numerical Analysis*, vol. **53**,  
887 no. 1, pp. 127–152, 2015.
- 888 Emery, A.H. and Lorenz, M., Thermal diffusion in a packed column, *Chemical Engineering*  
889 *Journal*, vol. **9**, no. 5, pp. 661–663, 1963.
- 890 Fargue, D., Jamet, P. and Costeséque, P., Dispersion phenomena in thermal diffusion and  
891 modelling of thermogravitational experiments in porous media, *Transport in porous*  
892 *media*, vol. **30**, no. 3, pp. 323–344, 1998.
- 893 Fargue, D., Costeséque, P., Jamet, P. and Girard-Gaillard, S., Separation in vertical  
894 temperature gradient packed thermodiffusion cells: an unexpected physical explanation



- 895 to a controversial experimental problem, *Chemical Engineering Science*, vol. **59**, no. 24,  
896 pp. 5847–5852, 2004.
- 897 Grillo, A., Lampe, M. and Wittum, G., Modelling and Simulations of Temperature-  
898 Density-Driven Flow and Thermodiffusion in Porous Media, *Journal of Porous Media*,  
899 vol. **14**, no. 8, pp. 671–690, 2011.
- 900 Gurtin, M.E., Fried, E. and Anand, L., *The Mechanics and Thermodynamics of Continua*,  
901 New York, USA: Cambridge University Press, 2010.
- 902 Gurtin, M.E., Generalized Ginzburg-Landau and Cahn-Hilliard equations based on a  
903 microforce balance, *Physica D*, vol. **92**, pp. 178–192, 1996.
- 904 Harinath Reddy, S., Raju, M.C. and Keshava Reddy, E., Soret and Dufour effects on  
905 radiation absorption fluid in the presence of exponentially varying temperature and  
906 concentration in a conducting field, *Special Topics & Reviews in Porous Media — An*  
907 *International Journal*, vol. **7**, no. 2, pp. 115–129, 2016.
- 908 Hassanizadeh, S.M., Derivation of basic equations of mass transport in porous media,  
909 Part 2. Generalized Darcy’s and Fick’s laws, *Adv. Water Resour.*, vol. **9**, pp. 207–222,  
910 1986.
- 911 Ingle, S.E. and Horne, F.H., The Dufour Effect, *J. Chem. Phys.*, vol. **59**, no. 11, pp.  
912 5882–5894, 1973.
- 913 Jamet, D., Diffuse interface models in fluid mechanics, *Adv. Water Resour.*, vol. **25**, no.  
914 3, pp. 335–348, 2001.
- 915 Jamet, P., Fargue, D., Costeséque, P., de Marsily, G. and Cernes, A., The thermogravita-  
916 tional effect in porous media: A modelling approach, *Transport in Porous Media*, vol.  
917 **9**, pp. 223–240, 1992.
- 918 Jasnow, D. and Vinals, J., Coarse-grained description of thermo-capillary flow, *Physics*  
919 *of Fluids A*, vol. **8**, pp. 660–669, 1996.

- 920 Joseph, D.D., Huang, A. and Hu, H., Non-solenoidal velocity effects and Korteweg stresses  
921 in simple mixtures of incompressible fluids, *Physica D*, vol. **97**, pp. 104–125, 1996.
- 922 Kita, R., Wiegand, S. and Luetttmer-Strathmann, J., Sign change of the Soret coefficient  
923 of poly(ethylene oxyde) in water/ethanol mixtures observed by thermal diffusion forced  
924 Rayleigh scattering, *Journal of Chemical Physics*, vol. **121**, no. 8, pp. 3874–3885, 2004.
- 925 Landau, L.D. and Lifschitz, E.M., *Fluid Mechanics, Second Edition: Volume 6 (Course*  
926 *of Theoretical Physics) 2nd edition*, UK: Pergamon, 1984.
- 927 Lorenz, M. and Emery, A.H., The packed thermal diffusion column, *Chemical Engineering*  
928 *Science*, vol. **11**, pp. 16–23, 1959.
- 929 Lowengrub, J. and Truskinovsky, L., Quasi-incompressible Cahn-Hilliard fluids and topo-  
930 logical transitions, *Proc. R. Soc. Lond. A*, vol. **454**, pp. 2617–2654, 1998.
- 931 Madariaga, J.A., Santamaria, C., Barrutia, H., Mounir Bou-Ali, M., Ecenarro, O. and Va-  
932 lencia, J.J., Validity limits of the FJO thermogravitational column theory: Experimen-  
933 tal and numerical analysis, *Comptes Rendus Mécanique*, vol. **339**, no. 5, pp. 292–296,  
934 2011.
- 935 Mallikarjuna, B., Chamkha, A.J. and Bhuvana Vijaya, R., Soret and Dufour effects on  
936 double diffusive convective flow through a non-Darcy porous medium in a cylindrical  
937 annular region in the presence of heat sources, *Journal of Porous Media*, vol. **17**, no.  
938 7, pp. 623–636, 2014.
- 939 Mićunović, M.V., *Thermodynamics of Viscoplasticity – Fundamentals and Applications*,  
940 New York, USA: Springer, 2009.
- 941 Nasrabadi, H., Hoteit, H. and Firoozabadi, A., An analysis of species separation in a  
942 thermogravitational column filled with a porous medium, *Transport in Porous Media*,  
943 vol. **67**, pp. 437–486, 2007.
- 944 Oldenburg, C.M. and Pruess, K., Layered Thermohaline Convection in Hypersaline  
945 Geothermal Systems, *Transport in Porous Media*, vol. **33**, pp. 29–63, 1998.

- Oldenburg, C.M. and Pruess, K., Layered Plume separation by transient thermohaline convection in porous media, *Geophysical Research Letters*, vol. **26**, no. 19, pp. 2997–3000, 1999.
- Platten, J.K., The Soret Effect: A Review of Recent Experimental Results, *Journal of Applied Mechanics*, vol. **73**, pp. 5–15, 2006.
- Quintard, M., Kaviany, M. and Whitaker, S., Two-medium treatment of heat transfer in porous media: numerical results for effective properties, *Adv. Water Resour.*, **20**, nos. 2–3, pp. 77–94, 1997.
- RamReddy, Ch., Murthy, P.V.S.N., Rashad, A.M. and Chamkha, A.J., Soret effect on stagnation-point flow past a stretching/shrinking sheet in a nanofluid-saturated non-Darcy porous medium, *Special Topics & Reviews in Porous Media — An International Journal*, vol. **7**, no. 3, pp. 229–243, 2016.
- Rauch, J., Diffusion and thermal diffusion in polymer solutions, PhD, Universität Bayreuth, Germany, 2006 (In German).
- Rauch, J. and Köhler, W., Diffusion and thermal diffusion of semidilute to concentrated solutions of polystyrene in toluene in the vicinity of the glass transition, *Phys. Rev. Lett.*, vol. **88**, no. 18, pp. 185901-1–185901-4, 2002.
- Rauch, J. and Köhler, W., Collective and thermal diffusion in dilute, semidilute, and concentrated solutions of polystyrene in toluene, *The Journal of Chemical Physics*, vol. **119**, no. 22, pp. 11977–11988, 2003.
- Rosanne, R., Paszkuta, M., Tevissen, E. and Adler, P.M., Thermodiffusion in compact clays, *Journal of Colloid and Interface Science*, vol. **267**, no. 1, pp. 194–203, 2003.
- Rowley, R.L. and Horne, F.H., The Dufour Effect. III. Direct experimental determination of the heat of transport of carbon tetrachloride-cyclohexane liquid mixtures, *J. Chem. Phys.*, vol. **72**, no. 1, pp. 131–139, 1980.

- 971 Salsa, S., *Partial Differential Equations in Action – From Modelling to Theory*, Milan,  
972 Berlin, Heidelberg, New York: Springer, 2008.
- 973 Srinivasacharya, D. and Kaladhar, K., Soret and Dufour effects on mixed convection flow  
974 of couple stress fluid in a non-Darcy porous medium with heat and mass fluxes, *Journal*  
975 *of Porous Media*, vol. **17**, no. 2, pp. 93–101, 2014.
- 976 Srinivasan, S. and Saghir, M.Z., Thermodiffusion in Multicomponent Mixtures—  
977 Thermodynamic, Algebraic, and Neuro-Computing Models, *Springer Briefs in Ther-*  
978 *mal Engineering and Applied Science (New York: Springer)*, vol. **106**, no. 9, 2013. DOI:  
979 10.1007/978-1-4614-5599-8.
- 980 Swernsath, S., Malengier, B. and Pushpavanam, S., Effect of Korteweg stress on viscous  
981 fingering of solute plugs in a porous medium, *Chemical Engineering Science*, vol. **65**,  
982 pp. 2284–2291, 2010.
- 983 Tyrrell, H.J.V., The calculation of diffusion coefficients and Soret coefficients from optical  
984 measurements on pure Soret effect cells, *Trans. Faraday Society*, vol. **52**, pp. 940–948,  
985 1956.
- 986 Veeresh, C., Varma, S.V.K., Raju, M.C. and Rushi Kumar, B., Thermal diffusion effects  
987 on unsteady magnetohydrodynamic boundary layer slip flow past a vertical permeable  
988 plate, *Special Topics & Reviews in Porous Media — An International Journal*, vol. **7**,  
989 no. 1, pp. 43–55, 2016.
- 990 Yadav, D. and Kim, M.C., The onset of transient Soret-driven buoyancy convection in  
991 nanoparticle suspensions with particle-concentration-dependent viscosity in a porous  
992 medium, *Journal of Porous Media*, vol. **18**, no. 4, pp. 369–378, 2015.
- 993 Yue, P., Feng, J.J., Liu, C. and Shen, J., A diffuse-interface method for simulating two-  
994 phase flows of complex fluids, *J. Fluid Mech.*, vol. **515**, pp. 293–317, 2004.
- 995 Zhang, K.J., Briggs, M.E., Gammon, R.W., Sengers, J.V. and Douglas, J.F., Thermal  
996 and mass diffusion in a semidilute good solvent-polymer solution, *Journal of Chemical*  
997 *Physics*, vol. **111**, no. 5, pp. 2270–2282, 1999.

998

## List of tables

Quantity	Units	HDO-H <sub>2</sub> O	C <sub>24</sub> H <sub>50</sub> -C <sub>12</sub> H <sub>26</sub>
$L$	m	$4.0 \cdot 10^{-1}$ [1]	$4.0 \cdot 10^{-1}$ [1]
$H$	m	$4.0 \cdot 10^{-3}$ [1]	$4.5 \cdot 10^{-3}$ [1]
$\phi$	—	0.4 [1]	0.4 [1]
$\varrho_0$	kg/m <sup>3</sup>	989.10 [2]	758.30
$c_0$	—	$5.8 \cdot 10^{-6}$	0.15
$T_{\text{ref}}$	°C	47.5 [1]	48.5 [1]
$\Delta T$	°C	19 [1]	25 [1]
$\beta$	1/K	$4.4 \cdot 10^{-4}$ [2]	—
$\gamma$	—	0	—
$\mu$	Pa · s	$5.7 \cdot 10^{-4}$ [2]	$0.96 \cdot 10^{-3}$ [1]
$\bar{D} = D/\phi$	m <sup>2</sup> /s	$2.09 \cdot 10^{-9}$ [2]	$6.5 \cdot 10^{-10}$ [1]
$S_{\text{st}}$	1/K	$6.3158 \cdot 10^{-5}$ [2]	$1 \cdot 10^{-3}$ [3]
$C_{\text{pf}}$	J/(kg · K)	4180.1 [2]	1094.7
$C_{\text{ps}}$	J/(kg · K)	1000.0 [4]	1000.0 [4]
$\kappa$	W/(m · K)	$\in [2.89, 9.27]$ [2]	$\approx 13$

Table 1:  $\bar{D} = 6.5 \cdot 10^{-10}$  m<sup>2</sup>/s refers to C<sub>24</sub>H<sub>50</sub>.  $S_{\text{st}} = 6.3158 \cdot 10^{-5}$  K<sup>-1</sup> is obtained by dividing  $S = 1.2 \cdot 10^{-3}$  (Benano-Melly et al., 2001) by  $\Delta T = 19$  K. [1] Jamet et al. (1992); [2] Benano-Melly et al. (2001); [3] Fargue et al. (1998); [4] Oldenburg and Pruess (1999).

Quantity	Units	C <sub>24</sub> H <sub>50</sub>	C <sub>12</sub> H <sub>26</sub>
True mass densities	kg/m <sup>3</sup>	$\varrho_1 = 799.1$	$\varrho_2 = 751.1$
Initial concentrations	kg/m <sup>3</sup>	$\chi_1 = 113.8$	$\chi_2 = 644.9$

Table 2: Experimental values taken from Jamet et al. (1992).

$\lambda$ [m <sup>4</sup> /s <sup>2</sup> ]	$S_{\text{st}}$ [1/K]	$S_{\text{eff,max}}$ [1/K]	$S_{\text{eff,min}}$ [1/K]
1.8	$3.5 \cdot 10^{-4}$	$6.39 \cdot 10^{-4}$	$2.13 \cdot 10^{-4}$
3.0	$2.0 \cdot 10^{-4}$	$5.73 \cdot 10^{-4}$	$6.81 \cdot 10^{-5}$
3.8	$1.2 \cdot 10^{-4}$	$5.04 \cdot 10^{-4}$	$7.14 \cdot 10^{-6}$

Table 3: Values corresponding to the curves in Figure 2d (cf. Fargue et al. (1998)).

999

## Figure Captions

1000

Figure 1: (a) Isolines of the solute mass fraction during the time, from the early times (left)

1001

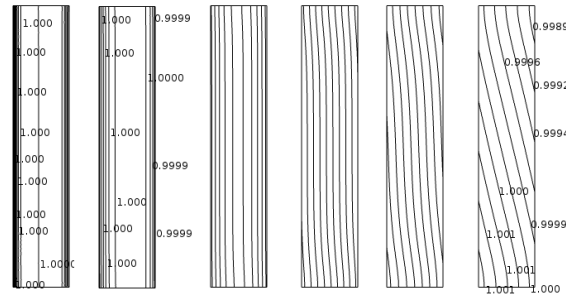
to the steady state (right). The results are obtained for the HDO-H<sub>2</sub>O mixture within the

standard setting of thermodiffusion. The benchmark is taken from Benano-Melly et al. (2001) and has been recomputed in the present paper with parameters  $L = 0.02$  m,  $H = 0.004$  m, and permeability  $k = 5 \cdot 10^{-12}$  m<sup>2</sup> (cf. Jamet et al. (1992)). (b) Spatial Pattern of  $S_{CH}$  for  $\lambda = 1.8$  m<sup>4</sup>/s<sup>2</sup> and  $k = 5 \cdot 10^{-12}$  m<sup>2</sup>, and the corresponding normalised mass fraction at the steady state. (c) Spatial Pattern of  $S_{CH}$  for  $\lambda = 1.8$  m<sup>4</sup>/s<sup>2</sup> and  $k = 1 \cdot 10^{-10}$  m<sup>2</sup>, and its corresponding normalised mass fraction at the steady state.

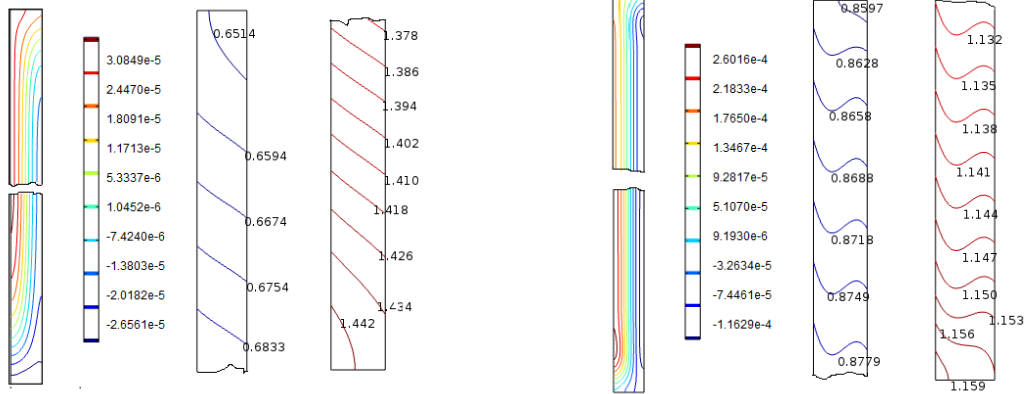
Figure 2: (a) Separation ratio as a function of permeability for the HDO-H<sub>2</sub>O mixture. (b) Separation ratio as a function of permeability for the C<sub>24</sub>H<sub>50</sub>-C<sub>12</sub>H<sub>26</sub> mixture. The results are obtained within the standard setting of thermodiffusion,  $\lambda = 0$  m<sup>4</sup>/s<sup>2</sup>. (c) Mixture HDO-H<sub>2</sub>O: Results obtained with standard Soret coefficient equal to  $S_{st} = 1.0 \cdot 10^{-5}$  1/K. (d) Mixture C<sub>24</sub>H<sub>50</sub>-C<sub>12</sub>H<sub>26</sub>: Results obtained for various values of  $\lambda$  and  $S_{st}$ . Best fit obtained for  $S_{st} = 2.55 \cdot 10^{-4}$  1/K. Experimental data and analytical curves have been recomputed and redrawn from Jamet et al. (1992) and Fargue et al. (1998).

Figure 3: (a) Steady state separation ratio for different values of  $\lambda$  in the HDO-H<sub>2</sub>O mixture (see also Jamet et al. (1992) and Fargue et al. (1998) for comparison). The standard Soret coefficient,  $S_{st}$ , is defined in Table 1. (b) Time evolution of  $\varepsilon$  for  $k = 8 \cdot 10^{-11}$  m<sup>2</sup>. (c) Dependence of  $\varepsilon$  on the permeability for some nonzero values of  $\lambda$ .

Figure 4: Mixture C<sub>24</sub>H<sub>50</sub>-C<sub>12</sub>H<sub>26</sub>. (a) Time behaviour of  $c_B$  (solid lines) and  $c_T$  (dashed lines), starting from a non-uniform mass fraction. Circled lines correspond to simulations involving  $S_{CH} \neq 0$  ( $\lambda = 3.8$  m<sup>4</sup>/s<sup>2</sup>) and  $S_{st} = 0$ . Lines with asterisks correspond to simulations in which  $S_{st} = 1.2 \cdot 10^{-4}$  1/K and  $S_{CH} = 0$ . Lines with no markers correspond to the case with no cross effects. (b) Initial mass fraction.

1027 **List of figures**

(a)



(b)

(c)

Figure 1

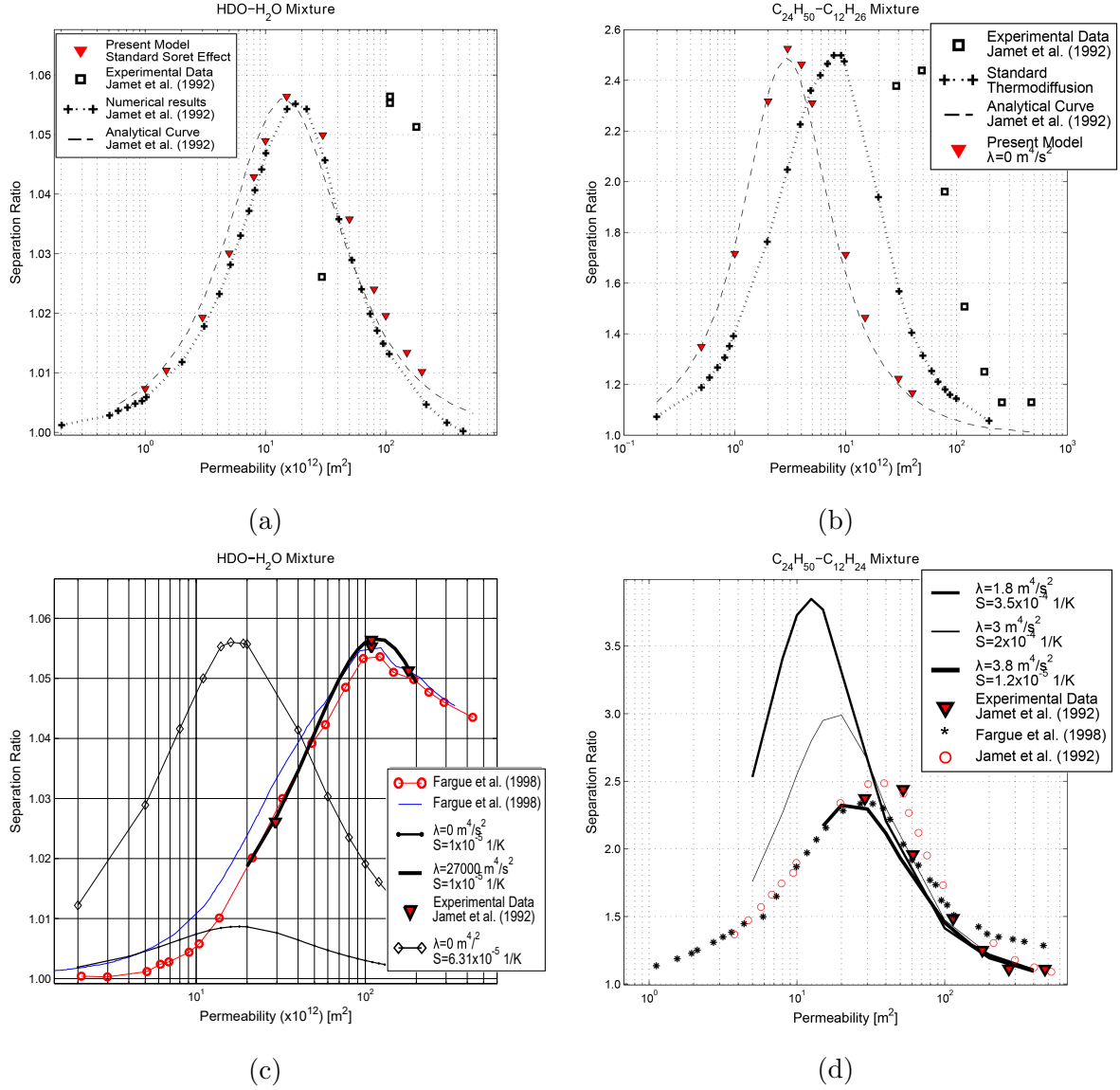
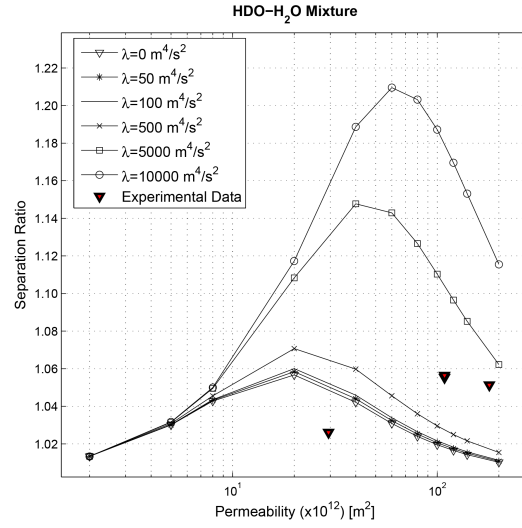
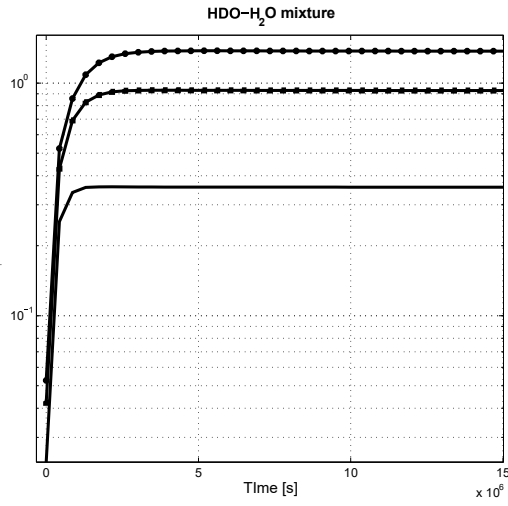


Figure 2

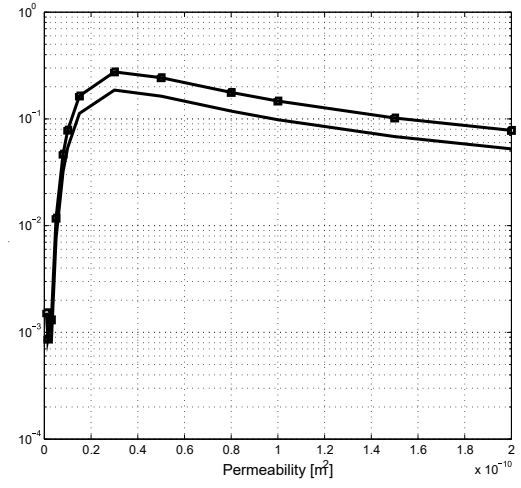




(a)

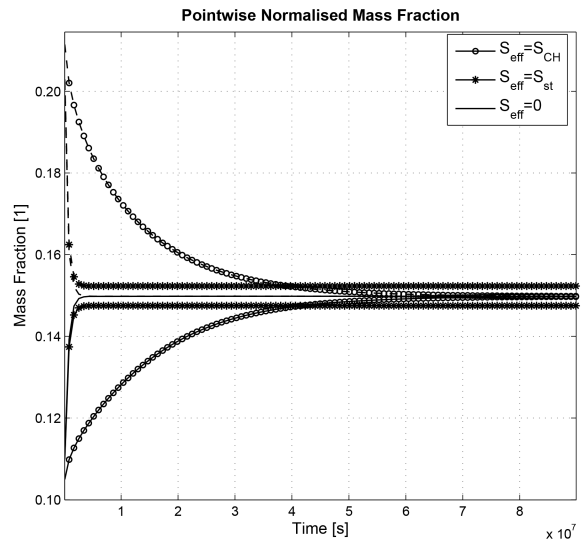


(b)

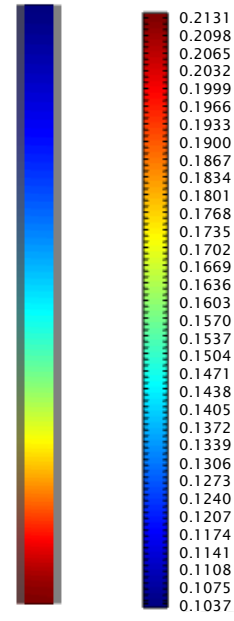


(c)

Figure 3



(a)



(b)

Figure 4